Characterization of Nicotiana benthamiana subtilisin-like peptidases

Vrkić, Ana

Master's thesis / Diplomski rad

2021

Degree Grantor / Ustanova koja je dodijelila akademski / stručni stupanj: **University of Zagreb, Faculty of Food Technology and Biotechnology / Sveučilište u Zagrebu, Prehrambeno-biotehnološki fakultet**

Permanent link / Trajna poveznica: https://urn.nsk.hr/urn:nbn:hr:159:510496

UNIVERSITY OF ZAGREB
FACULTY OF FOOD TECHNOLOGY AND BIOTECHNOLOGY

GRADUATE THESIS

Zagreb, September 2021

Ana Vrkić
1030/MB

CHARACTERIZATION OF *Nicotiana benthamiana* SUBTILISIN-LIKE PEPTIDASES

Experimental research for this thesis was conducted at the Department of Applied Genetics and Cell Biology, University of Natural Resources and Life Sciences, Vienna, under the mentorship of professor Lukas Mach, PhD. Experiments were performed with the guidance of Alejandro A. Puchol Tarazona, PhD.

I would like to express my sincere gratitude to professor Lucas Mach for the opportunity to work on my master's thesis in his laboratory and for all of his professional guidance.
I would like to thank Alejandro Puchol for his patience and extensive assistance during all of my experiments.
I want to extend my gratitude to all the members of the laboratory for making my short stay an invaluable experience.

Zahvaljujem profesorici Kseniji Durgo na pristupačnosti i vrijednim savjetima.

Hvala mojim prijateljima na nezaboravnim iskustvima tijekom ovih godina.

I na kraju, veliko hvala mojoj obitelji na beskonačnoj podršci i razumijevanju.

BASIC DOCUMENTATION CARD

Graduate Thesis

University of Zagreb
Faculty of Food Technology and Biotechnology
Department of Biochemical Engineering
Laboratory for Biology and Microbial Genetics

Scientific area: Biotechnical Sciences
Scientific field: Biotechnology

Characterization of *Nicotiana benthamiana* subtilisin-like peptidases

Ana Vrkić, 1030/MB

Abstract: Despite its many advantages, production of recombinant proteins in plants often encounters low yields, mainly due to proteolytic degradation by endogenous peptidases. *Nicotiana benthamiana*, a promising expression platform for production of human biologics is no exception. It was previously found that broadly neutralizing antibodies (bnAbs) against type 1 human immunodeficiency virus (HIV-1) (2F5, PG9) undergo proteolytic degradation when expressed in *N. benthamiana* leaves, and recently, two subtilisin-like serine peptidases were found to be responsible for the majority of those cleavage events. In this thesis, two Nb subtilases (NbPhyt1 and NbP69F) suspected to be involved in proteolysis of anti-HIV-1 bnAbs *in planta*, were characterized. It was shown that *in vitro* NbPhyt1 cleaves the PG9 heavy chain at the third complementarity determining region (CDRH3), at the same position as the Ab is cleaved *in planta* ($NYYD^{112}\downarrow F^{113}YDG$). The enzyme is most reactive towards the Ab at pH 4.0-5.5, which is in accordance with the enzyme's activity in the apoplastic fluid (pH~5.5). NbPhyt1 activity towards PG9 was best inhibited by fluorophosphonate-biotin (FP-biotin) and N-acetyl-YVAD chloromethyl ketone (Ac-YVAD-CMK), then 4-(2-aminoethyl)benzenesulfonyl fluoride hydrochloride (AEBSF) and benzyloxycarbonyl-VAD fluoromethyl ketone (Z-VAD-FMK). The collected data strongly suggest that NbPhyt1 participates in processing of PG9 *in planta*.

Keywords: *Nicotiana benthamiana*, monoclonal antibody, peptidase
Thesis contains: 70 pages, 19 figures, 13 tables, 109 references, 1 appendix
Original in: English
Graduate Thesis in printed and electronic (pdf format) **version is deposited in:** Library of the Faculty of Food Technology and Biotechnology, Kačićeva 23, Zagreb.

Supervisor at home faculty: *Ksenija Durgo, Full professor, PhD*
Principal supervisor: *Lukas Mach, Full professor, PhD*
Technical support and assistance: *Alejandro A. Puchol Tarazona, PhD*

Reviewers:
1. PhD. *Igor Stuparević*, Associate professor
2. PhD. *Ksenija Durgo*, Full professor
3. PhD. *Ivana Radojčić Redovniković*, Full professor
4. PhD. *Anamarija Štafa*, Assistant professor (substitute)

Thesis defended: 30 September 2021

TEMELJNA DOKUMENTACIJSKA KARTICA

Diplomski rad

Sveučilište u Zagrebu
Prehrambeno-biotehnološki fakultet
Zavod za biokemijsko inženjerstvo
Laboratorij za biologiju i genetiku mikroorganizama

Znanstveno područje: Biotehničke znanosti
Znanstveno polje: Biotehnologija

Karakterizacija peptidaza sličnih subtilizinu iz biljke *Nicotiana benthamiana*

Ana Vrkić, 1030/MB

Sažetak: Unatoč mnogim prednostima biljaka u proizvodnji rekombinantnih proteina, njihov najveći nedostatak je nizak prinos proizvoda za koji su uglavnom odgovorne biljne endogene peptidaze. S istim se problemom susreće i *Nicotiana benthamiana*, obećavajući domaćin za proizvodnju rekombinantnih ljudskih proteina. Prethodno je pokazano da neutralizirajuća antitijela protiv virusa humane imunodeficijencije tipa 1 (HIV-1) (2F5, PG9) podliježu razgradnji prilikom proizvodnje u listovima ove biljke, te je nedavno utvrđeno da su za proteolizu velikim dijelom odgovorne dvije subtilizinu slične serinske peptidaze (subtilaze). U ovom radu su okarakterizirane dvije Nb subtilaze (NbPhyt1 i NbP69F) za koje se sumnja da sudjeluju u proteolizi neutralizirаćih anti-HIV-1 antitijela *in planta*. Rezultati pokazuju da, *in vitro*, NbPhyt1 cijepa teški lanac PG9 antitijela u trećoj regiji koja određuje komplementarnost (CDRH3), na istom mjestu kao i kod antitijela proizvedenog *in planta* (NYYD^{112}↓F^{113}YDG). Najveća aktivnost NbPhyt1 je utvrđena pri pH 4.0-5.5, što je u skladu s aktivnosti enzima u apoplastu (pH~5.5). Najbolje inhibitorno djelovanje na aktivnost NbPhyt1 imali su fluorofosfonat-biotin (FP-biotin) i N-acetil-YVAD klorometil keton (Ac-YVAD-CMK), zatim 4-(2-aminoetil)benzensulfonil fluorid hidroklorid (AEBSF) i benziloksikarbonil-VAD fluorometil keton (Z-VAD-FMK). Prikupljeni rezultati snažno upućuju na to da NbPhyt1 sudjeluje u razgradnji PG9 antitijela *in planta.*

Ključne riječi: *Nicotiana benthamiana*, monoklonalno antitijelo, peptidaza
Rad sadrži: 70 stranica, 19 slika, 13 tablica, 109 referenci, 1 dodatak
Jezik izvornika: engleski
Rad je u tiskanom i elektroničkom obliku (pdf format) **pohranjen u:** Knjižnica Prehrambeno-biotehnološkog fakulteta, Kačićeva 23, Zagreb

Mentor na matičnom fakultetu: *prof.dr.sc. Ksenija Durgo*
Glavni mentor: *prof.dr.sc. Lukas Mach*
Pomoć pri izradi: *dr.sc. Alejandro A. Puchol Tarazona*

Stručno povjerenstvo za ocjenu i obranu:
1. Izv.prof.dr.sc. *Igor Stuparević*
2. Prof.dr.sc. *Ksenija Durgo*
3. Prof.dr.sc. *Ivana Radojčić Redovniković*
4. Doc.dr.sc. *Anamarija Štafa* (zamjena)

Datum obrane: 30. rujna 2021.

TABLE OF CONTENTS

1. INTRODUCTION

Molecular farming refers to large-scale production of proteins with potential pharmaceutical and/or commercial value via plant-based production platforms (Fischer and Emans, 2000). Even though bacterial and mammalian cells are still the most extensively used expression systems, plants offer many advantages, especially in terms of availability, product quality, safety and cost efficiency – a promising potential for production of both pharmaceutical and nonpharmaceutical recombinant proteins (Tschofen *et al.*, 2016). Among many plants available, *Nicotiana benthamiana* occupies a prominent position in molecular farming due to its rapid growth, high leaf biomass and prolific seed production. It is neither a food nor a feed crop so there is little risk of contamination of either food or feed chains. *N. benthamiana* is extremely susceptible to plant pathogens, a great advantage for establishing both stable and transient expression hosts (Twyman *et al.*, 2003; Bally *et al.*, 2018).

Due to competitiveness of conventional expression systems, plant-based platforms have focused on higher-added value biopharmaceuticals with three main product classes emerging: antibodies, vaccine candidates and replacement proteins (Schillberg *et al.*, 2019). Accordingly, therapeutic- and research-grade antibodies have been successfully produced in *N. benthamiana*, e.g. Abs against influenza, Ebola virus, HIV-1, hepatitis A/B/C virus, SARS coronavirus etc. (Powell, 2015).

HIV-1 is the causative agent of global epidemics of AIDS. Its potency lies in its extreme genetic variability arising from several factors (Hemelaar, 2012): multiple cross-species transfers, rapid replication and high mutation rates due to lack of proofreading by reverse transcriptase, intra-subtype recombination, inter-subtype recombination and generation of circulating recombinant forms (CRFs), development of antiviral drug resistance. Because of this, the neutralizing antibody response should be broad. So far, classical approaches to vaccine development (pathogen mimicry and particle-based vaccines) have been able to elicit only strain-specific and non-neutralizing antibodies (Burton *et al.*, 2012). Electrofusion hybridoma technology and phage display library systems enabled identification of *first generation* bnAbs; studies on b12, 2G12, 2F5 and 4E10 elucidated important HIV-1 vulnerability sites (Zhang *et al.*, 2016). These and similar Abs often have unusual features such as high levels of somatic mutation, long CDRH3 loops, polyreactivity and domain exchange (Burton *et al.*, 2012). Development of high-throughput neutralization assays

(Wu *et al.*, 2010), panels of diverse HIV-1 isolates and single B-cell cloning technology (Scheid *et al.*, 2009), as well as identification of individuals producing high titers of bnAbs (the *elite neutralizers*; Simek *et al.*, 2009), allowed for extensive analyses of Ab potency and target epitopes, and subsequently the discovery of a plethora of bnAbs.

Plant-produced recombinant proteins are often subjected to proteolytic degradation by endogenous peptidases. In order to improve yields, peptidases responsible for degradation of recombinant proteins must be well-characterized and appropriate measures taken, e.g., co-expression of inhibitors, gene knock-down/-out, or targeting to protease-poor subcellular compartments (Mandal *et al.*, 2016). Broadly neutralizing antibodies against HIV-1 undergo proteolytic cleavage when produced in *N. benthamiana* (Niemer *et al.*, 2014). The plant's leaf secretome contains a large number of serine, cysteine, aspartic and metallo peptidases (Grosse-Holz *et al.*, 2018a). Recently, two *N. benthamiana* apoplastic subtilases have been identified that participate in proteolysis of the bnAbs 2F5 and PG9 (Puchol Tarazona *et al.*, 2021).

The main aim of this thesis is characterization of two *N. benthamiana* subtilases suspected to be involved in proteolytic degradation of broadly neutralizing antibodies against HIV-1 – NbPhyt1 and NbP69F. Firstly, NbPhyt1 and NbP69F will be transiently expressed in *N. benthamiana* leaves: gene(s) of interest will be integrated into the pEAQ expression vector and delivered into the leaf apoplast using *A. tumefaciens* (agroinfiltration). Newly synthesized NbPhyt1/NbP69F will be extracted from the leaf material and purified by affinity chromatography. Secondly, NbPhyt1/NbP69F activity will be tested by activity-based protein profiling using FP-biotin and biotinyl-YVAD-CMK probes. To test their degradation capacity, NbPhyt1/NbP69F will be incubated with bnAbs PG9, 2F5, 2G12-wt and 2G12-I19R. Further characterization of proteolytic activity will include pH and inhibition profiles. Finally, antibody cleavage sites will be analyzed by mass spectrometry.

2. LITERATURE REVIEW

2.1. PRODUCTION OF RECOMBINANT PROTEINS IN PLANTS

Plant-based production platforms show valuable advantages over their well-established counterparts, e.g. *Escherichia coli* and Chinese hamster ovary (CHO) cells, such as increased safety concerning endotoxins and viral contaminants, lower production costs with bioreactor-free facilities and inexpensive media, high scalability in either in-field or greenhouse cultivation, correct and homogenous posttranslational modifications, fast production with transient systems (Chen and Davis, 2016), to name a few. Major limitations to commercial exploitation of plant systems, however, arise from generally low expression levels of recombinant proteins in plants. To counter this, extensive research was/is conducted to generate efficient expression cassettes, prevent gene silencing, improve mRNA stability and translational efficiency, improve recombinant protein stability and optimize environmental factors (Desai *et al.*, 2010; Twyman *et al.*, 2013). Even with maximum levels of expression achieved, the final protein yield greatly depends on the efficiency of downstream processing. It is estimated that downstream processing for plant-derived pharmaceuticals, in order to meet GMP standards, accounts for ~80% of total production costs (Fischer *et al.*, 2013). A unique advantage of some plant-produced pharmaceuticals is the possibility of administration as partially processed or unprocessed plant material (e.g. oral delivery of vaccines). This greatly facilitates downstream processing and eliminates costly storage and transport requirements, thereby increasing availability of many biopharmaceuticals (Kwon and Daniell, 2015).

2.1.1. Expression methods

Plant expression systems utilize cell suspension cultures, transgenic plants and transient expression hosts. Cell cultures are suitable for high-grade cosmetic and research/diagnostic reagents required in small quantities. This platform is the costliest to establish and sustain due to bioreactors, strictly defined media, regulated environment and low product yields. Transgenic plants are ultimately the best choice in terms of long-term production, in-field cultivation and process scalability. Yields in whole plants can be improved by breeding and selection among the best performing primary transformants. Lastly, transient expression allows fast production of large quantities of the product

of interest and is especially useful for 'setting the stage' for development of transgenic production hosts (Tschofen *et al.*, 2016; Burnett and Burnett, 2020).

Stable expression

Development of transgenic plants, i.e. integration of gene(s) of interest into the host genome, is a demanding and time-consuming process, but is ultimately the platform of choice for lasting and reproducible production of recombinant proteins. Common methods for nuclear transformation are *A. tumefaciens* mediated (Hellens *et al.*, 2000) and particle mediated gene transfer (biolistics). Their downsides are arbitrary gene incorporation and gene silencing. This can be overcome with gene editing techniques such as Zinc-finger nucleases, transcription activator-like effector nucleases (TALEN) and the CRISPR/Cas9 system (Rozov and Deineko, 2019). Heterologous DNA can be introduced into plastid genomes as well. Due to high transgene copy numbers and absence of transgene silencing (Ma *et al.*, 2003), high concentrations of recombinant proteins with no adverse physiological consequences can be achieved (Bally *et al.*, 2011), as well as simultaneous expression of multiple genes (Desai *et al.*, 2010) and increased biosafety (Ruf *et al.*, 2007). A major limitation for production of human glycoproteins, however, is the absence of glycosylation pathways in plastids.

Transient expression

Transient expression refers to heterologous gene expression when the gene of interest is not integrated into the host's genome but remains in the host for only a limited period. Transient production is a method of choice in response to emergencies like pandemics, when rapid vaccine and drug development, production and distribution is crucial. Transiently expressed monoclonal antibodies are one of the most valuable pharmaceutical products of this technology, e.g. ZMapp, a mAb cocktail against Ebola virus disease that was successfully produced in *N. benthamiana* leaves (Qiu *et al.*, 2014). Transient systems are generated via plant pathogens – *A. tumefaciens* and plant viruses. The former is known as *agroinfiltration*. Here, the sequence of interest is placed within T-DNA borders and delivered into plant material by pressure (syringe) or vacuum infiltration of the bacterial suspension (Stoger *et al.*, 2014). The latter is termed *full virus* strategy and utilizes wild type viral vectors, e.g. tobacco mosaic virus. *Magnifection* (agroinfection)

combines the two – deconstructed viruses are introduced to plant cells by agroinfiltration. The method integrates beneficial elements of the viral machinery like RNA/DNA amplification, enhanced translation and cell-to-cell spread, with bacteria assuming the function of primary infection and systemic movement. Advantages of this system are fast process development and scale-up, high product yields and improved biocontainment (Gleba *et al.*, 2005).

2.1.2. Posttranslational modifications

Protein biosynthesis and secretory pathways are highly conserved between plants and animals, hence production of recombinant human proteins in plant expression systems is favored over yeast and bacterial ones. In this regard, co- and post-translational modifications (PTMs) are especially important as most eukaryotic proteins are modified during or after synthesis on ribosomes. For a large proportion of biopharmaceuticals, only a small subset of PTMs has so far been reported with glycosylation being the most complex and widespread (Walsh, 2010).

Glycan structures influence protein folding, stability, half-life, solubility, oligomerization and catalytic activity (Goettig, 2016). Early N-glycosylation steps that take place in the endoplasmic reticulum (ER) and *cis*-Golgi are virtually identical in higher eukaryotes, while differences arise further in glycan processing. Interestingly, only a small number of Golgi-processing enzymes were identified in plants that give rise to typically two major glycan structures. In contrast, more than a hundred enzymes are responsible for over two thousand glycan structures identified on mammalian proteins (Loos and Steinkellner, 2014).

Both plant and mammalian glycoproteins have identical N-glycan core structures but different terminal and side residues – plant complex N-glycans lack β(1,4)-galactose and sialic acid, carry core α(1,3)-fucose instead of α(1,6)-fucose and have β(1,2)-xylose residues (Figure 1). Proper glycosylation of recombinant proteins can be achieved *in planta* with metabolic glycoengineering approaches (Strasser *et al.*, 2014). Plants exhibit greater amenability to glycoengineering, as well as increased homogeneity of glycan structures over CHO cells, the most commonly used system for production of human therapeutics (Bosch *et al.*, 2013). For example, RNA interference (RNAi) technology was successfully used in *N. benthamiana* for production of mAbs lacking plant-specific glycan modifications (Strasser *et al.*, 2008).

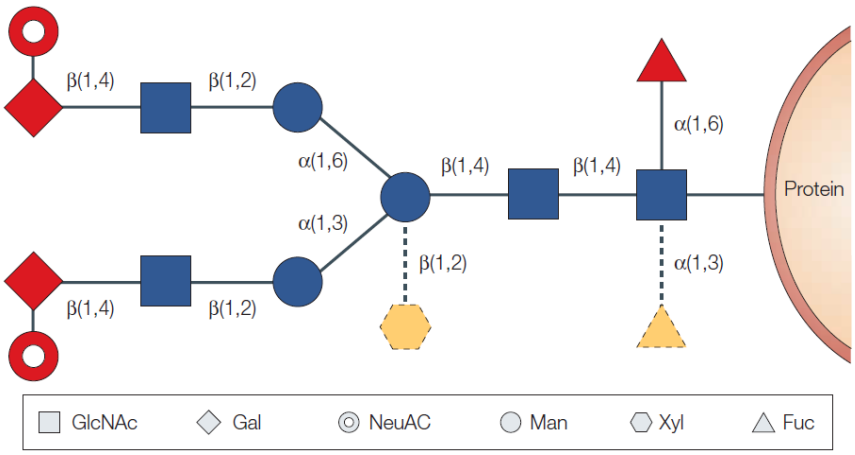

Figure 1. Complex glycan structures of plant and human proteins (Ma *et al.*, 2003): blue – residues common to both plants and humans, red – residues common to human proteins, yellow – residues common to plant proteins.

2.2. PEPTIDASES

Peptidases (proteases, proteinases) are protein hydrolases, enzymes that carry out hydrolysis of peptide bonds and irreversibly change their substrates. They are classified into families and clans according to the amino-acid sequence homology and tertiary structure similarities (common ancestor), respectively. According to the nature of their catalytic site, i.e. the chemical mechanism of hydrolysis, there are serine (S), cysteine (C), threonine (T), aspartic (A), glutamic (G), asparagine (N) and metallo- (M) catalytic type[1] peptidases. Additionally, based on the selectivity for the peptide bond, endopeptidases cleave internal peptide bonds and exopeptidases remove up to three residues from the N- (aminopeptidases) or C-terminus (carboxypeptidases) (Rawlings et al., 2018; Klein et al., 2018). Information on proteolytic enzymes, their substrates and inhibitors can be found in the *MEROPS* database (Rawlings *et al.*, 2018).

In general, peptidases polarize the carbonyl group of the substrate scissile bond making the carbon susceptible to attack by an activated nucleophile, such as hydroxyl or sulfhydryl groups of the active site Ser, Thr and Cys, or an activated water molecule in case of Asp, Glu and metallo-peptidases (van der Hoorn, 2008; López-Otín and Bond, 2008). Some peptidases are highly specific, while others have a broad range of substrates. Substrate specificity is determined by

[1] Additionally, peptidases can be classified as unknown (U) or mixed (P) catalytic type.

molecular interactions at the protein-protein (peptidase-substrate) interface in the peptidase's substrate binding cleft (Figure 2).

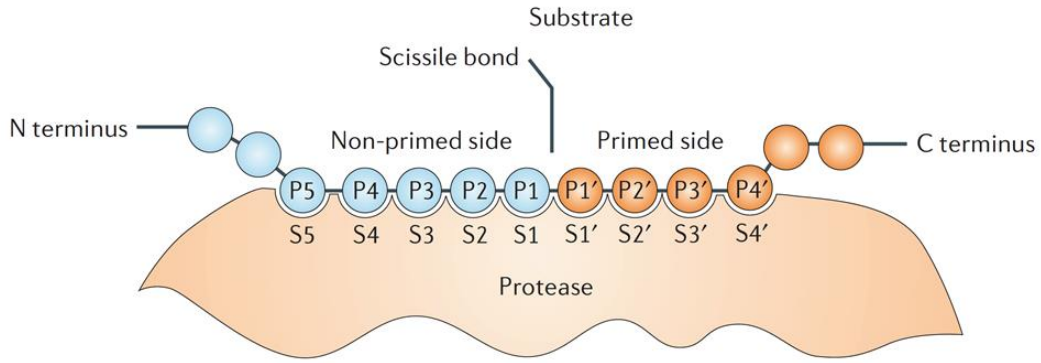

Figure 2. Schematic representation of peptidase-substrate interaction (Turk, 2006). Substrate amino acid side chains are marked starting from the scissile bond towards the N- (P1-Pn) or C-terminus (P1'-Pn'); peptidase subsites are marked accordingly (S1-Sn and S1'-Sn').

2.2.1. Plant specific peptidases

Peptidases have a myriad of physiologically and developmentally vital functions, from housekeeping to regulatory ones: degradation of redundant, damaged, misfolded and potentially harmful proteins and provision of amino acids for *de novo* protein synthesis (protein turnover), site-specific limited proteolysis as a means of zymogen maturation, alteration of protein activity, stability and localization, to name a few. Proteolysis is recognized as a vital regulator in all stages of the plant life cycle (Schaller, 2004; van der Hoorn, 2008). Plant genomes encode several hundred proteolytic enzymes localized in various subcellular compartments, while many are secreted to and active in the apoplast, a default destination for recombinant proteins targeted to the secretory pathway (Hehle *et al.*, 2011).

The largest peptidase classes in plants are of the Ser, Cys, metallo-, Asp and Thr catalytic type (Grosse-Holz *et al.*, 2018a).

Subtilisin-like serine peptidases

Subtilisin-like serine peptidases or subtilases (SBTs; S8 family, SB clan) are found in *Eukarya*, *Bacteria* and *Archaea*. They constitute the largest serine peptidase family in plants (Schaller *et al.*, 2018). The general structure of SBTs (SlSBT3 as a model) is shown in Figure 3.

Subtilases are synthesized as pre-pro-enzymes, with the N-terminal secretion signal peptide removed during co-translational translocation across the ER membrane. The prodomain is autocatalytically cleaved during zymogen maturation. It is required for proper folding of the enzyme and its autoinhibition through substrate-like binding to the catalytic subtilisin domain. Plant subtilases have a protease-associated (PA) domain inserted between the His and Ser residues of the Asp-His-Ser catalytic triad, and a C-terminal fibronectin (Fn)III-like domain (Schaller *et al.*, 2018). The former contributes to substrate recognition and selectivity, as well as homodimerization necessary for enzyme activation. The latter enhances enzyme stability and is functionally required for only some SBTs, e.g. SlSBT3. Unlike other subtilases, plant SBTs do not require calcium for thermostability (Cedzich *et al.*, 2009; Ottmann *et al.*, 2009).

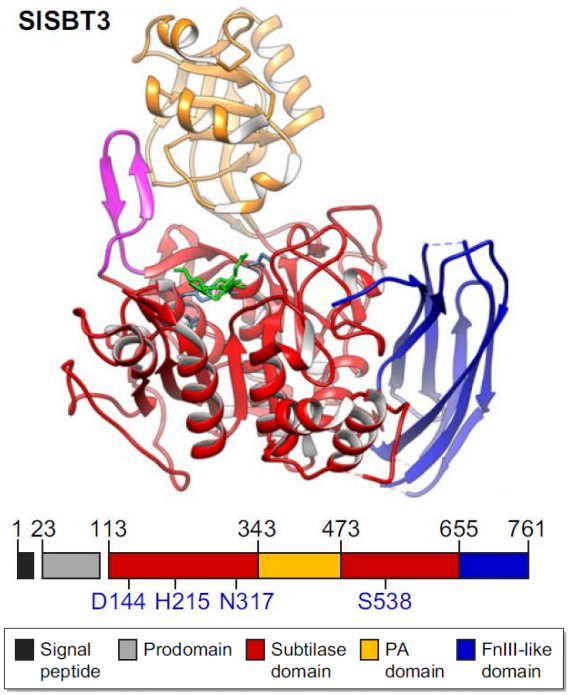

Figure 3. Structure of *Solanum lycopersicum* subtilase 3 (SlSBT3) (Schaller *et al.*, 2018).

Plant SBTs have been best studied in *Arabidopsis thaliana*, where the S08 family has 56 members. *Nicotiana benthamiana* also counts 56 SBTs, 28 of which were detected in the apoplastic fluid collected from agroinfiltrated leaves. Of these, 12 were among the 10% most abundant extracellular proteins (Grosse-Holz *et al.*, 2018a). Besides protein turnover, subtilases participate in specific processing of precursor proteins, generation of signalling peptides, formation of antimicrobial peptides, and are implicated in programmed cell death (PCD), pathogen defence and organism growth and development (Schaller *et al.*, 2018). Phytaspases are known to be involved in direct cleavage of target proteins, specifically after the aspartic acid residue. Although structurally unrelated, phytaspases exhibit functional similarities to animal caspases as they are involved in PCD, in particular the hypersensitive response induced by pathogen infection (Chichkova *et al.*, 2014). Tobacco phytaspase was found to be involved in plant protection during agrobacterium-mediated transformation, its target being the agrobacterial VirD2 protein that drives T-DNA transport into the nucleus (Reavy *et al.*, 2007). P69 SBTs are involved in pathogen defence as modulators of the plant immune responses. Tomato P69B and P69C are coordinately and systemically induced by pathogen infection. The latter was found to be involved in the remodeling of the extracellular matrix, possibly as a part of immune signaling (Schaller *et al.*, 2018).

2.2.2. Unwanted proteolysis of plant-produced recombinant proteins

A major problem encountered during recombinant protein production in plants is proteolytic degradation and subsequently significant reduction in product yield (Doran, 2006). It has been shown that proteolytic processing largely occurs along the secretory pathway and in the apoplast, a major drawback for production of recombinant glycoproteins such as monoclonal antibodies. Interestingly, degradation during downstream processing is not as significant (Hehle *et al.*, 2011). Recently, *N. benthamiana* SBT1 and SBT2 were shown to be involved in proteolysis of transiently expressed monoclonal antibodies (Puchol Tarazona *et al.*, 2021).

In vivo, peptidase activity is controlled by several mechanisms: regulation of gene expression, activation of inactive zymogens, blockade by endogenous inhibitors, subcellular targeting, glycosylation, metal binding, S-S bridging and proteolysis (López-Otín and Bond, 2008). Approaches to counter unwanted proteolysis of plant-produced recombinant proteins are discussed in the following section.

Peptidase inhibitors

Since peptidases irreversibly change their substrates, their activity *in vivo* must be strictly regulated. This is accomplished with peptidase inhibitors that either block the enzymes' activity by substrate-like binding to the active site, prevent substrate access by binding to regions adjacent to the active site or allosterically alter the conformation of the active site and thus decrease the enzymes' affinity for the substrate (Turk, 2006). Many peptidase inhibitors are multifunctional and/or have a relaxed specificity, i.e. one inhibitor can interact with multiple enzymes (Grosse-Holz and van der Hoorn, 2016). Co-expression of peptidase inhibitors with the protein of interest is a powerful approach to reduction of unwanted proteolysis in plants (Rivard *et al.*, 2006). For example, increase in yield of IgG complexes was achieved in *N. tabacum* roots by co-expression of a Bowman-Birk Ser peptidase inhibitor (Komarnytsky *et al.*, 2006); co-expression of *Sl*CYS8, a member of tomato cystatin family, resulted in substantial increase in accumulation of murine C5-1 (Robert *et al.*, 2013) and VRC01 Abs (Grosse-Holz *et al.*, 2018 b) in *N. benthamiana* leaves.

Gene knock-down/out

Unwanted proteolytic degradation of recombinant proteins can be prevented by targeting peptidase-encoding genes and/or their transcripts. RNAi or post-transcriptional gene silencing (PTGS) technology utilizes sequence-specific small dsRNAs to target mRNAs for degradation by the RNA-induced silencing complex (RISC) (Sontheimer, 2005). Using this technology a Cys peptidase in rice was silenced and recombinant protein synthesis thus increased (Kim *et al.*, 2008). Also, a stringently controlled, chemically inducible RNAi system was produced in transgenic *A. thaliana* and *N. benthamiana* (Guo *et al.*, 2003), a great advantage when working with indispensable proteins. Another antisense RNA technology utilizes ssRNAs that complementary bind mRNA and inhibit translation by disrupting ribosome binding or recruiting RNaseH (Bennett and Swayze, 2010). It was successfully used in tobacco BY-2 cells to simultaneously silence four genes encoding peptidases of different catalytic classes (Mandal *et al.*, 2014). Complete gene disruption (*knockout*) is possible using precision genetic modification techniques such as CRISPR/Cas, TALENs, ZFNs etc. (Fichtner *et al.*, 2014). This strategy, however, might prove futile if the target proteases are indispensable for plant growth and development.

Protein targeting

In order to obtain high yields of stable and active protein, retention in selected cellular compartments via protein targeting is employed. The ER lumen, for example, is advantageous over apoplast and cytosol owing to its highly oxidizing environment with abundance of chaperones and comparatively few proteases (Ma *et al.*, 2003). Fusion with γ-zein N-terminal domain enables protein accumulation in the form of ER-derived protein bodies, leading to e.g. an increase in yield of subunit vaccine F1-V from *Yersinia pestis* produced in *N. benthamiana* leaves and *N. tabacum* NT-1 suspension cells (Alvarez *et al.*, 2010). A major disadvantage of protein retention in the ER, however, is the absence of late PTMs, e.g. complex-type glycosylation taking place in the Golgi (Benchabane *et al.*, 2008). Another class of protein bodies in seeds are protein storage vacuoles (PSVs). Compared to lytic vacuoles that are rich in hydrolytic enzymes, PSVs provide a mild environment well adapted for protein accumulation and storage (Stoger *et al.*, 2005).

Stabilizing agents

Designing recombinant variants with improved stability (e.g. removing peptidase susceptible sites and/or integrating stabilizing conserved sequences) is difficult within the existing regulatory framework for therapeutics since maximal identity between the recombinant protein and its original counterpart is required (Benchabane *et al.*, 2008). Alternatively, protein-stabilizing agents like BSA (James *et al.*, 2000), PVP (Sharp and Doran, 2001), gelatin (Kwon *et al.*, 2003) etc., can be supplemented to culture suspensions to enhance and maintain recombinant protein stability without changing its primary structure. This, however, complicates the purification process and increases downstream processing costs.

2.3. ANTIBODIES

Antibodies (Ab) or immunoglobulins (Ig) are glycoproteins bound to the surface of and secreted by B-lymphocytes. The main functions of antibodies are neutralization of infectivity, phagocytosis, antibody-dependent cellular cytotoxicity (ADCC) and complement-mediated lysis of pathogens or infected cells (Forthal, 2014).

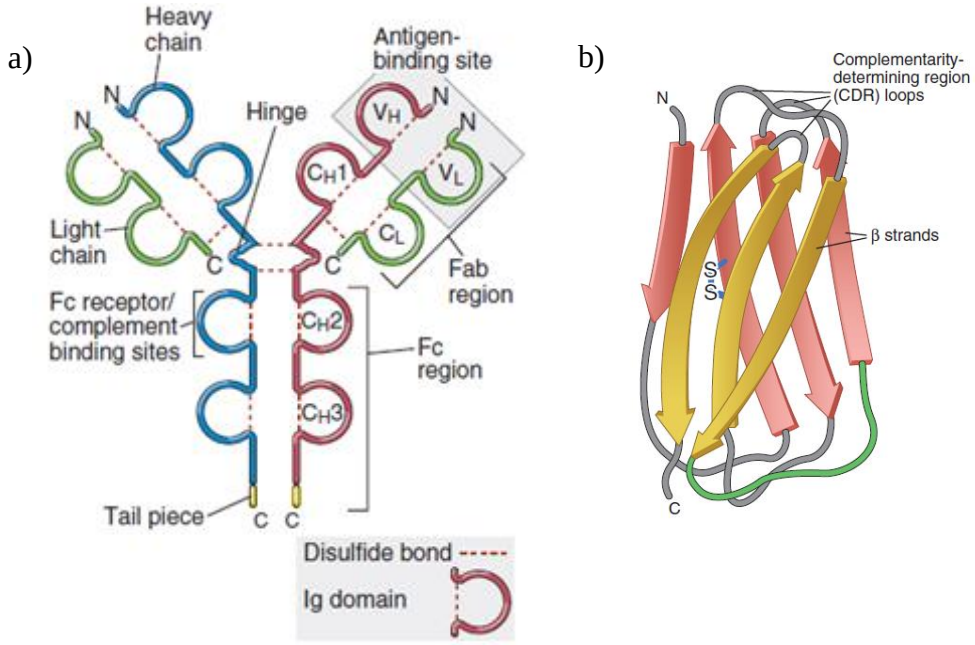

Figure 4. Structure of: a) secreted IgG molecule, b) Ig variable domain (Abbas et al., 2011).

As shown in Figure 4, Abs are composed of two identical copies of light (L) and heavy (H) chains: the L chain consists of one variable (V_L) and one constant (C_L) region; the H chain comprises one variable (V_H) and three (or four) constant (C_H) regions. The N-terminal domains of the L and H chains associate to form the Fab domain, carrying the antigen recognition/binding site, while the C-terminal parts of the H chains form the Fc domain that mediates cellular and molecular effector functions. Each V/C region folds independently in a globular motif called an Ig domain. V_H and V_L domains contain three hypervariable complementarity-determining regions (CDRs) each, distributed between the less variable framework (FW) regions. Six CDRs constitute the antigen-binding site, determining antigen complementarity and Ab specificity. Among these, CDRH3 is the most diverse in structure and size (Goldsby *et al.*, 2003; Abas *et al.*, 2011). According to the differences in their C_H regions, five classes/isotypes of human Abs arise. Fabs and Fc of IgG, IgA

and IgD are connected by the flexible *hinge* – region rich in Pro, Thr and Ser, containing disulfide bonds between the H chains and enabling lateral and rotational movement of Fabs (Lipman *et al.*, 2005) – while IgE and IgM possess another C_H domain instead (Goldsby *et al.*, 2003; Abas *et al.*, 2011).

2.3.1. Broadly neutralizing monoclonal antibodies against HIV-1

The HIV-1 viral envelope is composed of a phospholipid bilayer with transmembrane (gp41) and surface (gp120) glycoproteins generated upon endoproteolytic cleavage of the highly glycosylated gp160 polyprotein precursor. Upon cleavage, gp120 and gp41 remain non-covalently associated as heterodimers, three copies of which form the envelope spike/knob (Env) (Pantophlet and Burton, 2006). Env defines viral tropism, mediates the fusion process and is the main target of Ab-mediated immune responses. Figure 5 shows Env epitopes targeted by potent bnAbs, all discussed in the following section.

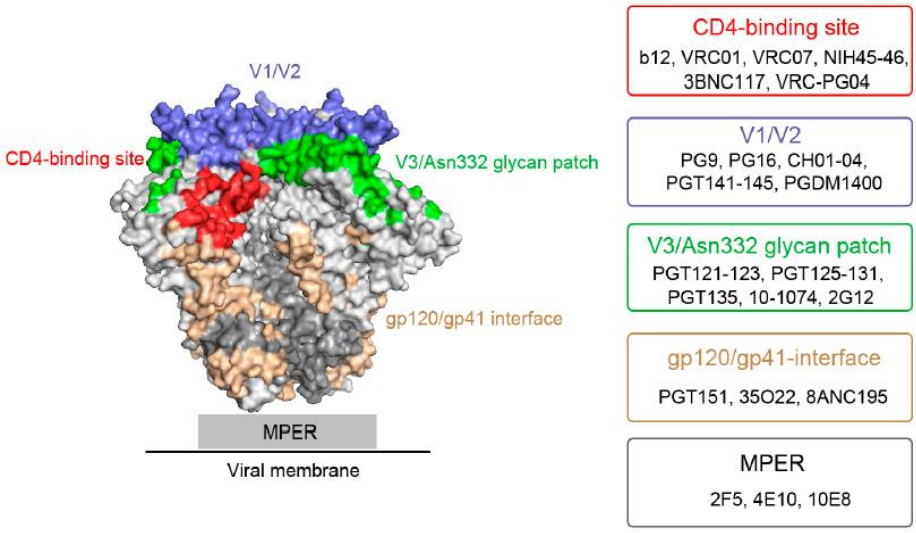

Figure 5. HIV-1 Env epitopes targeted by bnAbs (Zhang *et al.*, 2016)

Abs to CD4-binding site

The HIV-1 CD4 binding site (CD4bs) is a conserved conformational epitope responsible for CD4 receptor binding, the primary HIV-1 target. CD4 binding induces exposure of the chemokine receptor (CCR5/CXCR4)-binding site and of the gp41 fusion peptide (Mao *et al.*, 2012). In contrast to the prefusion state, CD4-bound Env displays more glycan-free, conserved surfaces,

therefore eliciting appropriate Ab responses more easily (Pancera *et al.*, 2014). Still, CD4bs has limited accessibility due to its position near the interprotomer interface and shielding by nearby V loops and glycans of its own and adjacent protomers (Ward and Wilson, 2015).

Anti-CD4bs Abs fall into two distinct categories: CDRH3-dominated and V_H-gene-restricted (Zhou *et al.*, 2015). VRC01 is a member of the latter, a CD4 mimetic that neutralizes over 90% of tested HIV-1 isolates. Apart from receptor mimicry, VRC01 owes its potency to the high degree of affinity maturation (Zhou *et al.*, 2010). The even more potent bnAb NIH45-46 was isolated from the same donor and has a four-residue insertion in CDRH3 acquired by somatic hypermutation, for interaction with the gp120 inner domain (Diskin *et al.*, 2011). CDRH3-dominated Abs are represented by the CH103 clonal lineage (Liao *et al.*, 2013). The main interaction with gp120 is accomplished by the CDRH3 loop. b12 was the first member of this group to be characterized (Burton *et al.*, 1994). Abs targeting CD4bs by non-CD4 mimetic mechanisms are generally less potent and more selective than CD4 mimetics (West *et al.*, 2014) due to the high mutability of V_H-germline genes that guides Ab maturation (Bonsignori *et al.*, 2016).

Abs to variable regions 1 and 2 (V1/V2)

HIV-1 variable loops mask the more conserved regions underneath, tolerate high mutation rates and are heavily glycosylated and flexible. Such are the V1 and V2 loops connecting the strands of the antiparallel β-sheet of the V1/V2 domain. They extend away from the trimer apex, with V1 projecting toward the high-mannose patch on the gp120 outer domain and V2 situated above the CD4bs (McLellan *et al.*, 2011; Ward and Wilson, 2015).

V1/V2-directed bnAbs have long protruding anionic tyrosine sulfated CDRH3s, assume β-hairpin conformation and are capable of penetrating an *N*-linked glycan shield to reach the cationic protein surface (McLellan *et al.*, 2011). Somatically related PG9 and PG16 Abs managed to neutralize 70-80% of circulating HIV-1 isolates. They show preferential trimeric spike binding and recognize a conformational epitope formed from conserved regions of the V1/V2 (and V3) loops (Walker *et al.*, 2009). Essential for their neutralization efficacy is interaction with the N-linked glycan Asn160 positioned centrally in the V2 loop. With its 28 residue-long CDRH3, PG9 engages with 5 out of 7 sugar moieties of the Asn160 $Man_5GlcNAc_2$. Interaction with other surface glycans, such as Asn156 and Asn173 is also important for Ab recognition and binding. PG9 and PG16 differ in

their preference for N-glycans, the latter being more sensitive to changes in viral glycosylation (Doores and Burton, 2010).

Abs to variable region 3 (V3)

V3 is a 35-residue long, highly variable and heavily glycosylated region of gp120 that plays a central role in HIV-1 tropism, i.e. the CCR5/CXCR4 coreceptor specificity (Hartley et al., 2005). Sequence variation is restricted to ~20% of its residues, primarily within the crown of the loop. Deletion of V3 completely abrogates virus infectivity (Zolla-Pazner and Cardozo, 2010). Epitope masking is reported for V3 by V1/V2 (Liu *et al.*, 2011).

PGT121 and 10-1074 are clonal variants that target a conserved epitope involving the N-glycosylation site at Asn332 and the base of V3. Both have 24-residue long CDRH3s with a nonpolar tip that may allow access to cryptic epitopes (Julien *et al.*, 2013; Mouquet *et al.*, 2012).

BnAb 2G12 recognizes a cluster of high-mannose glycans ($Man_{8\text{-}9}GlcNAc_2$) and binds terminal Manα1,2Man-linked sugars utilizing an unusual domain-exchanged structure. Its $(Fab)_2$ forms a multivalent binding surface that comprises two canonical antigen-binding sites (V_H/V_L) involving Asn332 and Asn392, and a third noncanonical binding site at the V_H/V_H' interface involving Asn339 (Calarese *et al.*, 2003; Doores *et al.*, 2010). Substitution of isoleucine with arginine at position 19 in the 2G12 heavy chain yields its nondomain-exchanged variant 2G12-I19R. This single residue substitution disables intramolecular Fab dimerization, rendering 2G12-I19R unable to recognize and bind said trimer glycan motifs (Doores *et al.*, 2010).

Abs to the membrane proximal external region (MPER)

The highly conserved MPER is positioned at the gp41 ectodomain C-terminus, connecting the ectodomain to the transmembrane domain. It contains highly conserved hydrophobic and Trp residues (Salzwedel *et al.*, 1999). Relevant to Ab neutralization, MPER has multiple structures which can be attributed to its structural flexibility, i.e. conformational changes during the fusion process (Barbato *et al.*, 2003).

2F5 has a sterically exposed, 22-residue long CDRH3 (Niemer *et al.*, 2014) and recognizes a gp41 MPER epitope containing (primarily) the amino acid sequence ELDKWA with additional contiguous residues important in stabilization of fusion transition conformations (Barbato *et al.*,

2003). More reactive towards MPER is 4E10 that recognizes the post-fusion coiled-coil structure (Kwong and Mascola, 2012) with its 18-residue long CDRH3, rich in Gly and Trp accounting for its flexibility and hydrophobic nature, respectively. Only two residues are in contact with the epitope, while others enable interactions with the viral membrane and/or other gp41 residues (Cardoso *et al.*, 2005). 10E8 binds MPER more efficiently than both 2F5 and 4E10. With its 22-residue long CDRH3, 10E8 recognizes an epitope overlapping the 4E10 epitope, with additional, crucial binding to Asn671 and Arg683 (Huang *et al.*, 2012).

Abs to the gp120/41 interface

PGT151 recognizes only cleaved, trimeric Env. Its interaction with the gp120/41 interface is glycan dependent – important for neutralization are conserved glycans at gp41 Asn611 and Asn637 (Falkowska *et al.*, 2014). Further, PGT151 recognizes a conserved, complex-glycan-dependent, quaternary epitope involving the gp120/gp41 interface of one protomer and one or more complex glycans at gp41 HR2 of the adjacent protomer. With its 26-residue long CDRH3 extending into the interprotomer cavity, PGT151 neutralizes the virus by stabilizing the gp41 prefusion conformation and gp120/gp41 interactions, thereby preventing CD4-induced conformational changes and fusion (Blattner *et al.*, 2014). 8ANC195 inserts its entire HC variable region into a gap in the virus shield to form a large interface that involves >50% contacts to gp120 glycans, with the glycans attached to Asn243 and Asn276 being crucial for Ab binding. It thereby prevents conformational changes required for gp41-mediated fusion. Variants of 8ANC195 may be particularly valuable since its epitope does not overlap with the targets of CD4bs, V2, V3 or MPER Abs (Scharf *et al.*, 2014).

3. MATERIALS AND METHODS

3.1. MATERIALS

3.1.1. Buffers and solutions

TAE, pH 8.2	40 mM Tris-acetate 1 mM EDTA
Infiltration buffer, pH 5.6	10 mM MES 10 mM $MgSO_4$ 0.1 mM acetosyringone
Extraction/Wash buffer, pH 7.0	50 mM Na_2HPO_4/NaH_2PO_4 200 mM KCl 20 mM imidazole
Elution buffer, pH 7.0	50 mM Na_2HPO_4/NaH_2PO_4 200 mM KCl 250 mM imidazole
Final buffer, pH 7.0	50 mM Na_2HPO_4/NaH_2PO_4 200 mM KCl
Storage buffer, pH 7.0	50 mM Na_2HPO_4/NaH_2PO_4 200 mM KCl 0.02 % NaN_3
SDS-PAGE sample buffer	125 mM Tris/HCl, pH 6.8 10 mM DTE 1 % (w/v) SDS 10 % glycerol 0.01 % bromophenol blue

SDS-PAGE running buffer	0.025 M Tris 0.2 M glycine 0.1 % (w/v) SDS
(Gel) Destaining solution	50 % ddW 40 % methanol 10 % acetic acid
(Gel) Staining solution	Destaining solution 0.02 % Coomassie Brilliant Blue R-250
Transfer buffer (TOWBIN)	25 mM Tris 192 mM glycine 1 mM SDS 20 % (v/v) methanol
Ponceau S solution	3 % (v/v) trichloroacetic acid (TCA) 0.1 % (w/v) Ponceau S
Phosphate-buffered saline (PBS), pH 7.4	137 mM NaCl 2.7 mM KCl 8.1 mM Na_2HPO_4 1.9 mM KH_2PO_4
PBST	PBS 0.05 % (w/v) Tween 20
Blocking solution	PBS 0.02 % (w/v) NaN_3 3 % (w/v) bovine serum albumin (BSA) or 3 % (w/v) milk powder or 3 % biotin-free BSA[2]

[2] When working with biotinylated samples

Elution buffer, pH 3.0	0.1 M glycine/HCl
Neutralization buffer, pH 8.0	1 M Tris/HCl

3.1.2. Media

LB, pH 7.0	1 % (w/v) peptone 1 % (w/v) yeast extract 0.5 % (w/v) NaCl 0.1 % (w/v) D-glucose + 0.1 mg/mL Kan (DH10β) or 0.1 mg/mL Kan, 0.5 mg/mL Gen (UIA143)
LB agar	LB 1.5 % agar
SOC	2 % (w/v) tryptone 0.5 % (w/v) yeast extract 10 mM NaCl 2.5 mM KCl 10 mM $MgCl_2$ 20 mM D-glucose

3.1.3. Reagents

Primers were custom-synthesized by Sigma-Aldrich. Restriction enzymes and DNA-modifying enzymes were purchased from Promega, Fermentas or New England Biolabs. DNA and protein markers/ladders were purchased from Thermo Fisher Scientific and Fermentas. The enhanced chemiluminescence WB reagent (ECL) was purchased from Bio-Rad Laboratories. The activity-based probes FP-biotin and biotinyl-YVAD-CMK were purchased from Santa Cruz Biotechnology and Bachem, respectively.

Table 1. List of primers used in screening/sequencing (S) and cloning (C); forward (Fw) or reverse (Rv) orientation; the sequence encoding the added his-tag is underlined.

Primer	**Sequence (5'→ 3')**	**Purpose**
NbPhyt1_GA-Fw	GTTAAGCTTCTGTATATTCTGCCCAAA TTCGCGATGGCCAATTGTATTACTATG	C, S
NbPhyt1_GA-Rv	GAAAATTTAATGAAACCAGAGTTAAAGGCCTAGTG ATGGTGATGGTGATGCAGAGGATCCACTCTTATG	C,S
NbP69F_GA-Fw	GTTAAGCTTCTGTATATTCTGCCCAAA TTCGCGATGGGATTCTTGCAAATCCT	C, S
NbP69F_GA-Rv	GAAAATTTAATGAAACCAGAGTTAAAGGCCTAGTGA TGGTGATGGTGATGTTCCACTAACAATACTACTGC	C, S
pEAQ-Fw	TTCTTCTTCTTCTTGCTGATTGGT	S
pEAQ-Rv	GCACAGAAAACCGCTCACCAAACA	S
NbPhyt1-IntRv	CTTATTTGGATTGATACGGC	S
NbP69F-IntFw	CTAATTTCACGACCAAGTG	S

Table 2. List of restriction enzymes used in the cloning process (C) and restriction analysis (R).

Restriction enzyme	Restriction site	Purpose
*Age*I-HF	5'…A↓CCGGT… 3' 3'…TGGCC↑A… 5'	C
*Xho*I	5'…C↓TCGAG… 3' 3'…GAGCT↑C… 5'	C
*BamH*I	5'…G↓GATCC… 3' 3'…CCTAG↑G… 5'	R
*Pst*I	5'…CTGCA↓G… 3' 3'…G↑ACGTC… 5'	R

Table 3. List of antibodies/reagents used in Western blot detection.

1° Ab	Mouse-α-6xHis (Takara Bio, Inc.)
	Rabbit-α-SBT1 (Andreas Schaller, Swiss Federal Institute of Technology)
2° Ab	Goat-α-Mouse IgG-HRP (Jackson ImmunoResearch)
	Goat-α-Rabbit IgG-HRP (Jackson ImmunoResearch)
	Goat-α-Human IgG-HRP (Sigma-Aldrich)
Biotin detection	Streptavidin-HRP (Vector Laboratories, Inc.)

Table 4. List of antibodies used in Ab digest assays.

Antibody	Production host	Manufacturer/Provider
PG9	CHO	Polymun Scientific
2F5	CHO	Polymun Scientific
2G12-wt	CHO	Polymun Scientific
2G12-I19R	Nb	Yvonne Taubenschmid, BOKU Vienna (batch from 22.4.2016)

Table 5. List of inhibitors used in NbPhyt1 inhibitor profiling analysis.

Inhibitor	Stock concentration	Manufacturer
AEBSF	0.2 M	Carl Roth
PMSF	0.2 M	Sigma-Aldrich
FP-biotin	10 mM	Santa Cruz Biotechnology
Ac-YVAD-CMK	10 mM	Bachem
Z-VAD-FMK	10 mM	Bachem

3.1.5. Organisms

Escherichia coli DH10β

The *E. coli* DH10β strain was used due to advantages like fast propagation, high DNA transformation efficiency, ability to take up and stably maintain large plasmids (>10 kb) and lack of methylation-dependent restriction systems (Durfee *et al.*, 2008).
Transformed cells were grown in LB and on LB-agar plates supplemented with kanamycin (0.1 mg/mL) at 37°C (suspension continuously mixed on a shaker). Methods involving DH10β are described in chapters 3.2.2.-3.2.7.

Agrobacterium tumefaciens UIA143

The *A. tumefaciens* UIA143 strain is a *recA* mutant, derivative of strain C58 (*autC58 recA::EryJ40*(pAtC58)): deficient in DNA repair and recombination functions but retaining its ability to conjugally transfer and receive plasmids (Farrand *et al.*, 1989). It harbors a pMP90 Ti-helper plasmid containing a gene encoding GenR and an active *vir* region (Hamilton, 1997). Here, expression of *vir* genes was induced with the phenolic compound acetosyringone (0.1 mM).
Transformed cells were grown in LB and on LB-agar plates supplemented with kanamycin (0.1 mg/mL) and gentamycin (0.5 mg/mL) at 29°C (suspension continuously mixed on a shaker). Methods involving UIA143 are described in chapters 3.2.8. and 3.2.9.

Nicotiana benthamiana

N. benthamiana ΔXT/FT plants were used for recombinant protein expression. These glycoengineered species lack plant-specific α1,3-fucosylation *and* β1,2-xylosylation. They are generated by RNAi-mediated downregulation of endogenous *FucT* and *XylT* genes, in order to produce mAbs lacking plant-specific glycosylation (Strasser *et al.*, 2008).
Plants were grown at 24℃ with a 16-hour light, 8-hour dark photoperiod, for 4-5 weeks prior to agroinfiltration. Methods involving *N. benthamiana* are described in chapters 3.2.9. and 3.2.10.

3.1.4. Plasmids

The pEAQ plasmids are a series of small binary vectors designed for transient expression (Sainsbury *et al.*, 2009). Created from pEAQ-*HT*, pEAQ-IgA_{hc} (Göritzer *et al.*, 2017) was used to design pEAQ-NbPhyt1 and pEAQ-NbP69F expression vectors, as described in 3.2.2.-3.2.4.
pEAQ-*HT* is based on the CPMV-*HT* expression system that uses CPMV RNA-2 UTRs to direct expression of a gene of interest placed between the (minimal) CaMV 35S promoter and the NOS terminator. The 5'UTR is mutated (the *hypertrans*/*HT* mutations) such that the upstream AUG (161) codon is removed, which greatly enhances translational efficiency. Insertion of foreign genes in CPMV-*HT* expression cassettes is possible either by restriction-based enzyme cloning or by using the GATEWAY recombination system. The expression cassette is placed within the plasmid's T-DNA region defined by the right and left border (RB/LB) T-DNA repeats. The sequence encoding the P19 suppressor of gene silencing (prevention of host-induced foreign mRNA degradation) and the eukaryotic NeoR/KanR resistance gene (coding for aminoglycoside phosphotransferase; selection in plants) are also contained within the T-DNA borders. The vector backbone contains the prokaryotic KanR gene (selection in *E. coli* and *A. tumefaciens)*, the broad-host origin of replication *oriV* and *trfA* encoding the activator of *oriV* (Peyret and Lomonossoff, 2013).
Plasmid maps were created in SnapGene, as shown in Figure 6.

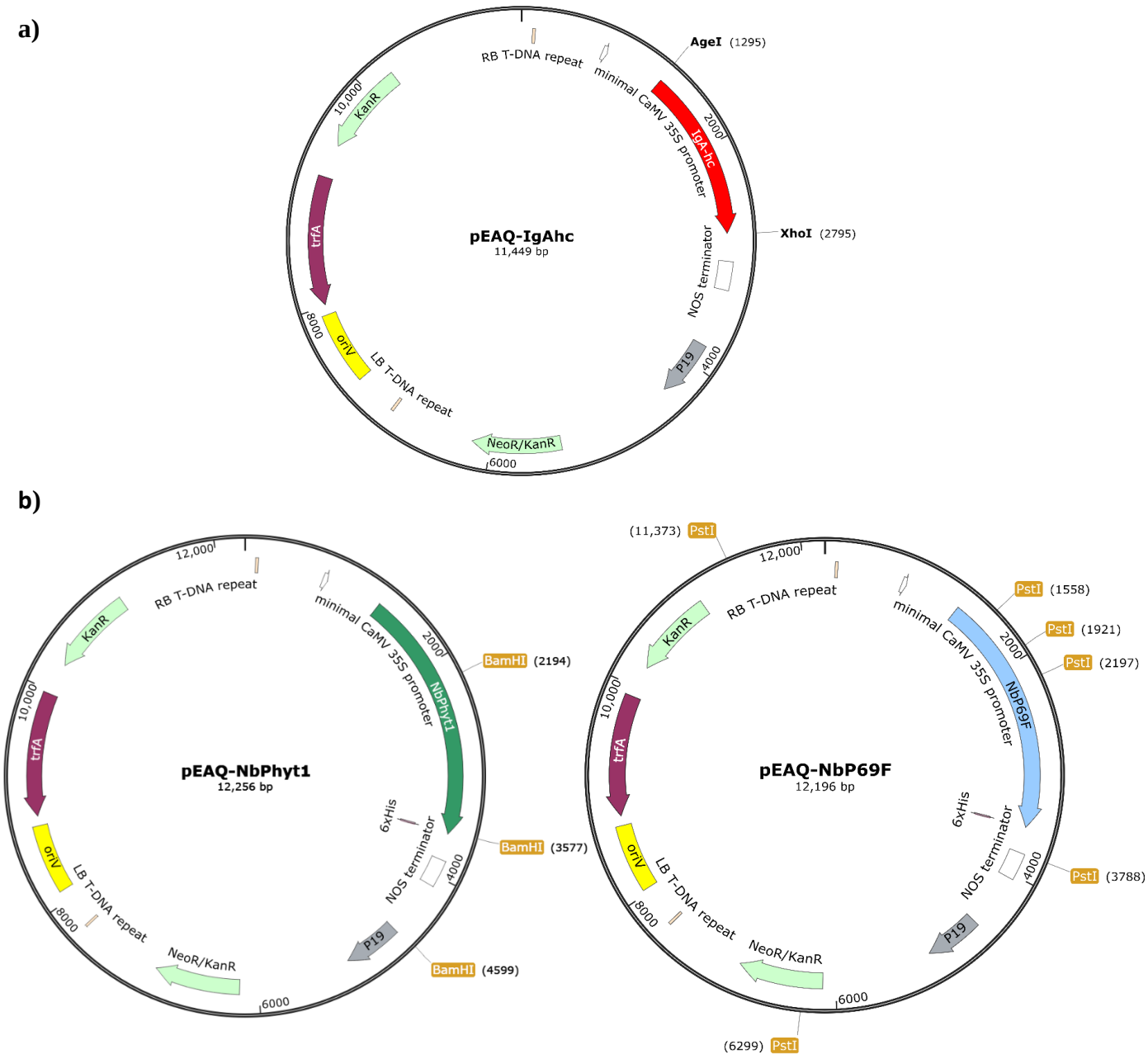

Figure 6. The plasmid backbone contains *oriV* (yellow), *trfA* (purple) encoding its activator and a prokaryotic KanR gene (light green). a) pEAQ-IgA_{hc}: positioned between LB and RB T-DNA repeats (light pink) are genes encoding IgA_{hc} (red), suppressor of gene silencing P19 (grey) and eukaryotic NeoR/KanR (light green). *Age*I and *Xho*I restriction sites are marked. b) pEAQ-NbPhyt1 (left) and pEAQ-NbP69F (right): like a) but with genes encoding NbPhyt1 (green) and NbP69F (blue) ligated into the *Xho*I and *Age*I restriction sites (instead of IgA_{hc}). Sites for *BamH*I (pEAQ-NbPhyt1) and *Pst*I (pEAQ-NbP69F) restriction analysis are highlighted (orange).

3.2. METHODS

3.2.1. Agarose gel electrophoresis

Agarose gel electrophoresis (AGE) was performed in all steps concerning DNA characterization. AGE separates DNA fragments according to their size. Smaller fragments migrate through the agarose gel faster than larger ones towards a positively charged electrode due to the negatively charged DNA backbone.

1 % agarose gels were prepared. To prepare a 40 mL gel, 0.4 g agarose was mixed with 40 mL TAE buffer in an Erlenmeyer flask and microwaved until completely dissolved. For detection of nucleic acids, 2 µL of (20000x) peqGREEN were added to the mixture. The mixture was poured into a gel tray and a sample well-comb was inserted (carefully to avoid air bubbles). The gel was allowed to solidify completely at room temperature (20-30 minutes). Next, the comb was carefully removed and the gel tray was transferred into an electrophoresis chamber. Prior to sample loading, the gel was completely submerged in TAE buffer. Samples were mixed with the appropriate amount of 6x loading dye (to visualize migration of DNA fragments) and loaded into sample wells. Gel electrophoresis was performed at 120 V/30 min. Bands were visualized with a UV transilluminator (GelDoc, Bio-Rad).

3.2.2. Isolation and restriction of pEAQ-IgA_{hc}

The pEAQ-IgA_{hc} plasmid was isolated and purified from an overnight DH10β culture using the Wizard Plus SV Minipreps DNA Purification System (Promega). The expression vector pEAQ was prepared by enzymatic restriction of pEAQ-IgA_{hc} with *Age*I-HF (New England Biolabs) and *Xho*I (Thermo Fisher Scientific). Restriction sites are shown in Table 2 and the reaction conditions are listed in Table 6. The amount of enzyme required for optimal restriction depends on the amount of plasmid DNA used and was determined according to the manufacturer's manual.

Table 6. Restriction of pEAQ-IgA_{hc}.

Restriction enzyme	Buffer	Reaction	Inactivation
*Age*I-HF	1x rCutSmart/1x Tango	37°C/2h30'	65°C/30'
*Xho*I	2x Tango	37°C/2h	80°C/20'

Double-digested (dd) pEAQ was separated from the IgA_{hc} fragment and remaining undigested plasmid by agarose gel electrophoresis. Bands corresponding to dd pEAQ were cut from the gel, followed by its purification using the Wizard SV Gel and PCR Clean-up System (Promega).

3.2.3. NbPhyt1 and NbP69F cDNA amplification

DNA sequences coding for the subtilisin-like serine proteases NbPhyt1 and NbP69F were previously cloned into the cloning vector pCR4. From this template, NbPhyt1 and NbP69F cDNAs were amplified by means of polymerase-chain-reaction (PCR) in a thermocycler. The PCR program used is shown in Table 7. Primer sequences are shown in Table 1.

Reaction:

0.5 µL DNA template	0.2µL Q5 polymerase
0.4 µL dNTPs (10 mM)	4.0 µL 5x Q5 buffer
1.0 µL Fw primer (10 µM)	12.9 µL ddW
1.0 µL Rv primer (10 µM)	
V_T = 20 µL	

Table 7. Amplification of NbPhyt1/NbP69F cDNA insert; PCR program.

cDNA insert			**NbPhyt1**	**NbP69F**
Primer combination			NbPhyt1_GA-Fw NbPhyt1_GA-Rv	NbP69F_GA-Fw NbP69F_GA-Rv
Program	Lid		105°C	
	1 – initial denaturation		98°C, 30''	
	2 – denaturation	x 35	98°C, 10''	
	3 – primer annealing		58°C, 25''	60°C, 25''
	4 – extension		72°C, 1'10''	
	5 – final extension		72°C, 5'	
	6 – end		10°C, 5'	

NbPhyt1/NbP69F cDNA inserts were purified using the Wizard SV Gel and PCR Clean-up System (Promega). Agarose gel electrophoresis and NanoDrop (Thermo Scientific) spectrophotometry were used to check their purity and determine the approximate DNA concentration.

3.2.4. Gibson Assembly

The NbPhyt1/NbP69F cDNA insert was subcloned into the dd pEAQ expression vector by Gibson Assembly (GA), an isothermal, single-tube reaction for assembling overlapping DNA molecules (Gibson et al., 2009). T5 exonuclease (thermolabile) removes nucleotides from 5' ends of dsDNA molecules. The resulting ssDNA overhangs anneal and Phusion DNA polymerase fills the gaps, while *Taq* DNA ligase joins the strands. A molar 1:2 to 1:3 vector to insert ratio was used for optimal reaction efficiency. Double-distilled (ddW) water was used instead of the insert as a negative control (later referred to as *GA without insert*).

Reaction:

3.6 µL 5x ISO buffer
0.25 µL Phusion polymerase
2.0 µL *Taq* ligase
2.0 µL T5 exonuclease (1:250 in ISO buffer)
X µL pEAQ vector
X µL NbPhyt1/NbP69F cDNA insert/ddW
X µL ddW
V_T = 20 µL

The reaction mixture was incubated in a thermocycler (lid preheated at 105°C) at 50°C/1 hour (cool-down at 10°C/10 min).

3.2.5. Production of electrocompetent DH10β

A baffled flask containing 500 mL sterile LB medium was inoculated with 2 mL of saturated overnight DH10β culture. The bacterial culture was incubated at 37°C/3 hours/100 rpm, that is until an OD_{600} of 0.5-0.7 was reached, indicating exponential phase of cell growth. Next, the cell suspension was incubated on ice at 4°C/1 hour and mixed by shaking every 10 minutes. The suspension was transferred to 250 mL GSA containers and centrifuged at 5000 rpm/4°C/15 min. The supernatant was discarded. The pellets were resuspended and washed in 200 mL cold ddW (centrifugation as above, supernatant discarded). Washing was repeated with 50 mL cold ddW and the contents of the two containers were combined (centrifugation as above, supernatant discarded). The last washing step was performed in 5 mL 10 % glycerol (centrifugation as above, supernatant discarded). Finally, the cell pellet was resuspended in 1 mL 10 % glycerol. 50 µL aliquots were transferred to 1.5 mL microcentrifuge tubes, snap-frozen in liquid nitrogen and stored at -70°C. The competency of the prepared cells was tested by electroporation with 1 ng of the plasmid pUC18. Transformed cells were plated on LB-agar plates (containing 0.1 mg/mL Ampicillin) and grown overnight at 37°C.

3.2.6. DH10β transformation

Competent DH10β *Escherichia coli* cells were transformed with Gibson assembly (GA) mixtures by electroporation. 50 µL frozen aliquots of electrocompetent DH10β were thawed on ice, mixed with 1 µL GA and transferred into cold cuvettes (2 mm electrode gap size). Electroporation was performed at 2.49 kV/5 msec (MicroPulser Electroporator, Bio-Rad). Immediately afterwards, cells were mixed with 950 µL sterile SOC medium, transferred to 1.5 mL microcentrifuge tubes and incubated at 37°C/1 hour/180 rpm. The cell suspension was then centrifuged at 16000 g/1 min, the cell pellet resuspended in 100 µL SOC and plated on LB-agar (0.1 mg/mL Kan) plates. Plates were incubated overnight at 37°C.

The following negative controls were set up: cells transformed with GA without insert, cells transformed with purified double digested pEAQ, untransformed cells.

3.2.7. Analysis of transformants – colony PCR and restriction analysis

Colonies were resuspended in 10 µL of sterile ddW and boiled at 95°C for 10 minutes in a thermocycler. Cooled suspensions were mixed with 15 µL colony PCR master mix.

Reaction:

2.5 µL Taq polymerase buffer
1.5 µL 25 mM $MgCl_2$
0.5 µL 10 mM dNTPs
1.25 µL forward primer (10 µM) 10 µL colony suspension
1.25 µL reverse primer (10 µM)
0.2 µL *Taq* polymerase
7.8 µL ddW

V_T = 25 µL

Colony PCR was performed in a thermocycler. Primer combinations and PCR program are shown in Table 8. Primer sequences are shown in Table 1. Amplified DNA fragments were separated and visualized by agarose gel electrophoresis.

Table 8. Colony PCR.

Sequence			**pEAQ-NbPhyt1**	**pEAQ-NbP69F**
Primer combination			pEAQ-Fw + NbPhyt1-IntRv	pEAQ-Rv + NbP69F-IntFw
Expected fragment size			~1.9 kb	~1.8 kb
Program	Lid		105°C	
	1		95°C, 1’	
	2	x 34	95°C, 20’’	
	3		45°C, 20’’	
	4		72°C, 2’	72°C, 2’30’’
	5		72°C, 10’	
	6		4°C, 5’	

For plasmid DNA isolation, 20 mL LB (containing 0.1 mg/mL Kan) medium was inoculated with PCR-positive colonies. Cells were grown at 37°C/overnight/180 rpm. Plasmid DNA was isolated and purified using the Wizard Plus SV Minipreps DNA Purification System. Restriction analysis (Table 9) of potential pEAQ-NbPhyt1/NbP69F clones was performed, followed by Sanger sequencing to verify positive results.

Table 9. Restriction analysis.

Restriction enzyme	*Bam*HI		*Pst*I	
Construct	**pEAQ-NbPhyt1**	**pEAQ-IgA$_{hc}$**		**pEAQ-NbP69F**
Fragment length (bp)	9851, 1383, 1022	11449	5074, 3864, 2511	5074, 2511, 2381, 1573, 363, 276

3.2.8. UIA143 transformation

Agrobacterium tumefaciens UIA143 cells were transformed with pEAQ-NbPhyt1/NbP69F (10-50 ng) by electroporation. 50 µL frozen aliquots of electrocompetent UIA143 were thawed on ice, mixed with pEAQ-NbPhyt1/NbP69F and transferred into cold cuvettes (2 mm electrode gap size). Electroporation was performed at 2.20 kV/5.2 msec. Immediately thereafter, cells were mixed with 950 µL sterile SOC medium, transferred to 1.5 mL microcentrifuge tubes and incubated at 29°C/2 hours/200 rpm. The cell suspension was centrifuged at 16000 g/1 min, the cell pellet resuspended in 100 µL SOC and plated on LB-agar (with 0.1 mg/mL Kan, 0.05 mg/mL Gen) plates. Plates were incubated at 29°C/2 days.

The following negative controls were set up: cells transformed with sterile ddW, untransformed cells.

3.2.9. Agroinfiltration of *N. benthamiana* leaves

4 mL of LB (0.1 mg/mL Kan, 0.05 mg/mL Gen) medium was inoculated with a single UIA143_pEAQ-NbPhyt1/NbP69F colony. Cells were incubated at 29°C/overnight/200 rpm. 300-400 µL of saturated culture was transferred to 20 mL LB (0.1 mg/mL Kan, 0.05 mg/mL Gen) medium and incubated at 29°C/overnight/200 rpm. The cell suspension was centrifuged at 4000 rpm/15 min/RT and the pellet resuspended in 30 mL infiltration buffer. The optical density at 600 nm was measured (expected between 3.0 and 4.0) and the suspension was diluted to OD_{600} = 0.15 and 300 mL total volume. Acetosyringone[3] was added at 0.1 mM final concentration just prior to leaf infiltration. Pressure infiltration with the bacterial suspension through the lower epidermis of the top 3-4 leaves was performed using a 1 mL disposable syringe (Figure 7).

The following negative controls were set up: leaves infiltrated with UIA143 w/o plasmid, uninfiltrated leaves.

Plants were incubated for 3 days at standard growth conditions (see 3.1.4).

Figure 7. *Nicotiana benthamiana* leaf infiltration (Ma *et al.*, 2012)

[3] Induction of Agrobacterium virulence genes.

3.2.10. Extraction of apoplastic fluid from *N. benthamiana* leaves

3 days post-infiltration *N. benthamiana* leaves were picked and submerged in an ice-cold extraction buffer, followed by vacuum exposure in a desiccator for ~15 minutes. The vacuum was then slowly released, resulting in buffer entry into the leaves' apoplast. Leaves were pat-dried from excess buffer, packed in multiples of three in gauze and placed in 50 mL centrifuge tubes (Greiner AG). Apoplastic fluid was extracted by centrifugation at 2000 rpm/15 min/4°C.

3.2.11. Affinity chromatography of his-tagged recombinant subtilases

Collected apoplastic fluid was loaded onto the IMAC column[4] (Ni-charged chelating sepharose fast flow) previously equilibrated in extraction buffer, and the flow-through was collected. Next, the column was equilibrated in wash buffer and 1 mL wash fractions were collected. The absorbance of the fractions was measured spectrophotometrically at 280 nm. When the absorbance value of the last wash fraction reached 0.01 and/or was not changing, elution of recombinant proteins followed. The column was equilibrated in elution buffer containing a high imidazole concentration for 15 minutes. Imidazole replaces histidine tags bound to the column, therefore eluting recombinant his-tagged proteins. 10 1 mL elution fractions were collected and their A_{280} was measured.

3.2.12. Buffer exchange and concentration of eluates

Eluate fractions with the highest A_{280} values were combined. Buffer exchange and concentration of the pooled eluate was performed using an ultrafiltration membrane (Microsep Advance Centrifugal Device). Elution buffer was exchanged with final buffer in a series of 6 centrifugation steps at +4°C and 7000 rpm, in each step (re)concentrating the sample from 5 mL to 500 µL. The final volume of the retentate was 150-200 µL.

[4] Immobilized metal ion affinity chromatography column; histidine forms a complex with immobilized Ni^{2+}

3.2.13. SDS-PAGE

Sodium dodecyl sulfate-polyacrylamide gel electrophoresis under reducing conditions was performed according to the Laemmli method. A discontinuous buffer system was used – stacking and separating gels were prepared as shown in Table 10. Samples were mixed with SDS-PAGE sample buffer and denatured at 95℃ for 5 minutes. A prestained marker protein ladder and the samples were loaded onto gels positioned vertically in an electrophoresis chamber filled with SDS-PAGE running buffer. Protein separation according to their size was performed at 200 V/1 hour. Gels were further used either for immunoblot analysis or Coomassie Brilliant Blue staining.

Table 10. Stacking and separating gel components.

Components	**Separating gel[5]**		**Stacking gel**
	12.7 %	**14.8 %**	**5.8 %**
30 % (w/v) acrylamide	3.5 mL	3.5 mL	650 µL
1 % (w/v) bisacrylamide	1.1 mL	1.05 mL	445 µL
1.5 M Tris/HCl pH 8.8	2.1 mL	1.825 mL	-
0.5 M Tris/HCl pH 6.8	-	-	850 µL
ddH_2O	1.6 mL	0.65 mL	1435 µL
10 % (w/v) SDS	84 µL	75 µL	35 µL
10 % (w/v) APS	50 µL	50 µL	25 µL
TEMED	5 µL	5 µL	2.5 µL

[5] Western blotting – 12.7 %, 10-well, 1.5 mm gels; Coomassie Brilliant Blue staining – 14.8 %, 10-well, 1.0 mm gels

3.2.14. Coomassie Brilliant Blue staining

Following SDS-PAGE, the gel was submerged in destaining solution at RT/30 min (protein fixation). Next, the gel was stained with Coomassie Brilliant Blue R-250 at RT/1 hour. To visualize protein bands only, the gel was destained as long as necessary to remove the stained background with several changes of the destaining solution.

3.2.15. Western blot (immunoblot) analysis

Proteins separated by SDS-PAGE were transferred onto a nitrocellulose membrane. The transfer system (*sandwich*) was assembled as shown below, and placed in a transfer chamber (Bio-Rad). Transfer[6] was performed for 1 hour at 100 V (PowerPac, Bio-Rad) in an ice-cold transfer buffer. Afterwards, membranes were blocked overnight in blocking solution at 4°C on a see-saw rocker. Antibodies used for Western blot detection are shown in Table 11. Blocked membranes were washed in PBST 3x for 5 minutes, and incubated in primary antibody solution for 1.5 hours at room temperature on a rocker. Membranes were washed in PBST 5x for 5 minutes prior to incubation in HRP (horseradish peroxidase)-conjugated secondary antibody solution, with the same conditions applied as during 1° Ab incubation. Blots were washed in PBST 3x for 5 minutes and rinsed twice in PBS, followed by chemiluminescence detection with ECL reagent. Protein bands were visualized on autoradiographic films in a dark room.

<u>Transfer system:</u>

Black side of the transfer cassette
Sponge
3 sheets of filter paper
SDS-PAGE gel
Nitrocellulose membrane
3 sheets of filter paper
Sponge
White side of the transfer cassette

[6] To confirm protein transfer, Ponceau S and Coomassie Brilliant Blue staining were performed on membranes and gels, respectively.

Table 11. Primary and secondary antibodies for Western blot detection.

Primary antibody	
Mouse-α-6xHis	1:5000 in PBST, 3% BSA, 0.02% NaN_3
Rabbit-α-SBT1	
Secondary antibody	
Goat-α-Mouse IgG-HRP	1:10000 in PBST, 0.5% BSA
Goat-α-Rabbit IgG-HRP	
Goat-α-human IgG-HRP	
Biotin detection	
Streptavidin-HRP	1:10000 in PBST, 0.5% biotin-free BSA

3.2.16. Identification of his-tagged recombinant subtilases

Recombinant NbPhyt1 and NbP69F were identified in total soluble protein extracts (TSP), apoplastic fluid (AF) and pooled (and concentrated) IMAC eluates by immunoblotting with antibodies against the 6xHis-tag and tomato SBT1 (for Abs see Table 12). Flow-through (FT) and final wash fractions (WX) collected during affinity chromatography of collected AFs, were also tested against α-6xHis and α-SBT1 antibodies. TSP and AF from leaves infiltrated with untransformed UIA143 (mock infiltration) were used as negative controls. Previously prepared TSP containing NbPhyt1 was used as a positive control.

3.2.17. Activity-based protein profiling

ABPP is a powerful functional proteomics technology. It takes advantage of small molecule probes that covalently and irreversibly label the active site of target enzymes in an activity-dependent manner (Morimoto and van der Hoorn, 2016).

Activity-based protein profiling (ABPP) of NbPhyt1/NbP69F was performed using activity-based probes (ABPs) FP-biotin and biotinyl-YVAD-CMK. The experiment was performed at pH 7.0.

NbSBT1 and NbSBT2 (isolated by Puchol Tarazona, 2019) were used as positive controls. Negative control samples contained ddW instead of activity-based probes.

Reaction:

18 µL enzyme
2 µL FP-biotin/biotinyl-YVAD-CMK (10 µM)/ddW
V_T = 20 µL

The reaction mixture was incubated at 37°C/1 hour. The reaction was then stopped by adding 7 µL of 4x SDS-DTE, followed by boiling at 95°C for 5 minutes. Western blot analysis was performed and biotin was detected with streptavidin-HRP .

3.2.18. *In vitro* antibody degradation assays

The activity of recombinant NbPhyt1 and NbP69F was tested towards four mAbs – PG9, 2F5, 2G12-wt and 2G12-I19R. Negative control samples contained final buffer instead of enzymes. The experiment was performed at pH 5.5.

Reaction:

5 µL enzyme/final buffer
2 µL PG9/2F5/2G12-wt/2G12-I19R (0.5 mg/mL)
10 µL NaAc (0.2 M, pH 5.2)
3 µL ddW
V_T = 20 µL (0.1 M NaAc, pH 5.5)

Reaction mixtures were incubated at 37°C. 3 µL aliquots for analysis were taken at t = 0, 30 minutes, 2 hours, 4.5 hours and overnight; t = 0 and overnight for negative control samples. Western blot detection of Abs' heavy chain and its degradation products was performed with Goat-α-human IgG_{hc}-HRP.

3.2.19. NbPhyt1 inhibitor profiling

The activity of NbPhyt1 towards PG9 and 2G12-I19R was also tested after pre-treatment with various inhibitors (Table 12). The negative control sample contained final buffer instead of enzyme. The positive control sample contained 1% DMSO instead of inhibitor. The experiment was performed at pH 5.5.

Table 12. List of inhibitors and their final concentrations used for NbPhyt1 inhibitor profiling.

Inhibitor	**Concentration**
AEBSF	20 mM, 1 mM
PMSF	1 mM
FP-biotin	100 µM
Ac-YVAD-CMK	100 µM
Z-VAD-FMK	100 µM

Reaction:

5 µL NbPhyt1/final buffer
2 µL inhibitor/DMSO
10 µL NaAc (0.2 M, pH 5.2)
1 µL ddW
2 µL PG9/2G12-I19R (0.5 mg/mL in PBS)

V_T = 20 µL (0.1 M NaAc, pH 5.5)

NbPhyt1 was incubated with inhibitors at 37°C/1 hour. Next, PG9 or 2G12-I19R was added. The reaction mixtures were incubated at 37°C/overnight, followed by western blot detection of the antibodies' heavy chain and its degradation products.

3.2.20. NbPhyt1 pH profiling

The activity of recombinant NbPhyt1 towards PG9 was tested at various pH values. McIlvaine buffers of appropriate pH – 4.0, 4.5, 5.0, 5.5, 6.0, 6.5, 7.0, 7.5 – were prepared using 0.1 M citric acid and 0.2 M Na_2HPO_4 (Table 13). The negative control sample contained final buffer instead of enzyme and 1xPBS instead of McIlvaine buffer.

Table 13. Preparation of McIlvaine buffers.

pH	**0.1 M citric acid (mL)**	**0.2 M Na_2HPO_4 (mL)**
4.0	30.7	19.3
4.5	27.5	22.5
5.0	24.3	25.7
5.5	21.8	28.2
6.0	18.4	31.6
6.5	14.8	35.2
7.0	8.8	41.2
7.5	4.1	45.9

Reaction:

2 µL NbPhyt1/final buffer

1 µL PG9 (0.5 mg/mL PBS)

7 µL McIlvaine buffer (pH 4.0-7.5)/PBS

V_T = 10 µL

Reaction mixtures were incubated overnight at 37°C, followed by western blot detection of PG9 and its degradation products.

3.3.21 PG9 cleavage site analysis

Identification of the PG9 cleavage site was performed by mass spectrometry. Preparation of the sample is described below. LC/MS was performed by Daniel Maresch of the Department of Chemistry, BOKU Vienna.

PG9 digest

In order to obtain a sufficient amount of Ab fragments for MS, it was necessary to scale up the Ab digest accordingly. Digestion of ~250 µg CHO-PG9 with NbPhyt1 was performed.

Reaction:

100 µL NbPhyt1
70 µL PG9 (3.62 mg/mL)
250 µL NaAc (0.2 M, pH 5.5)
130 µL ddW
V_T = 500 µL

The reaction mixture was incubated at 37°C for 1.5 days (2 nights) in total. Progress of the Ab digest was examined by SDS-PAGE and Coomassie Brilliant Blue gel staining.

Purification and buffer exchange

Digested PG9 was purified from the reaction mixture using protein-A sepharose beads, while maintaining a temperature of +4°C. 20 µL of a 50% bead-suspension in 20% EtOH were washed 3x with 500 µL PBS. The digested PG9 sample was transferred onto and mixed with the beads, followed by incubation at +4°C/2 hours on a rotator (ensuring slow and uniform mixing). Following incubation, the beads were left to settle and the supernatant was carefully removed. The beads were washed 4x with 500 µL PBS and then incubated for 5 minutes in 100 µL glycine eluent (pH 3.0) during which they were mixed by vortexing each minute. After the final spin-down and settling of the beads, 100 µL eluate was transferred into a clean tube and mixed immediately with 10 µL neutralization buffer (pH 8.0). 4 more eluates were collected (omitting the 5-minute incubation step). Buffer exchange and concentration of the pooled eluate (~550 µL) was performed

with a Microsep Advance Centrifugal Device (MW cut-off: 10K; Pall Corporation). Elution buffer was exchanged with PBS in a series of 6 centrifugation steps at 4800 rcf/+4°C/20 min by (re)concentrating the sample from 2 mL to ~200 µL in each step. Finally, the sample was concentrated to ~100 µL. Its A_{280} was measured via NanoDrop to estimate the protein concentration.

MS analysis

Antibodies and their degradation products were treated with PNGase F (Roche, Basel, Switzerland) at 37°C/16 hours to release their N-glycans, and reduced with 10 mM DTT at 56°C/45 min to separate Ab chains. A Thermo ProSwift RP-4H column (250 × 0.20 mm) using a Dionex UltiMate 3000 HPLC system (Thermo Fisher Scientific) was used for fractionation. After the sample application (5 µL), elution was performed at 65°C and a flow rate of 8 µL/min, with a gradient of 20-95% solvent B (80% acetonitrile in 0.01% trifluoroacetic acid) in solvent A (0.05% trifluoroacetic acid), over 40 min as follows: 20-65% B (15 min), 65-95% B (5 min). Eluted polypeptides were analysed online on a maXis 4G ETD Q-TOF mass spectrometer (Bruker) equipped with an electrospray ionization source and operated in the positive ion mode (m/z range: 400-3800). The analysis files were deconvoluted (Maximum Entropy Method) using DataAnalysis 4.0 (Bruker) and manually annotated.

4. RESULTS AND DISCUSSION

In this section, all relevant results of NbPhyt1 and NbP69F characterization, as well as those of preceding methods, are shown and discussed.

DNA related results: plasmid isolation and digestion, cDNA insert amplification, plasmid and insert purification, efficacy of Gibson assembly, colony PCR and restriction reactions were analyzed by agarose gel electrophoresis (shown as figures). Additional data on DNA purity and concentration was obtained by NanoDrop spectrophotometry (data not shown).

Protein related results: isolation and purification of recombinant subtilases was analyzed spectrophotometrically (shown as graphs), by staining of SDS-PAGE gels and by immunoblotting (shown as figures); Activity-based protein profiling, Ab digestion assays, inhibitor profiling and pH profiling were analyzed by immunoblotting; Ab cleavage site was analyzed by mass spectrometry.

4.1. PLASMID PRODUCTION FOR RECOMBINANT PROTEIN EXPRESSION

4.1.1 Cloning of NbPhyt1 and NbP69F

The DNA sequence coding for NbPhyt1/NbP69F was previously cloned into the cloning vector pCR4, from which it was amplified by PCR using Gibson assembly (GA) primers. pEAQ-IgA_{hc} was digested with *Age*I-HF and *Xho*I. Double-digested (dd) plasmid was loaded onto and cut out from an agarose gel. NbPhyt1/NbP69F cDNA and dd pEAQ were purified by use of the Wizard SV Gel and PCR Clean-up System, followed by ligation via the GA method.

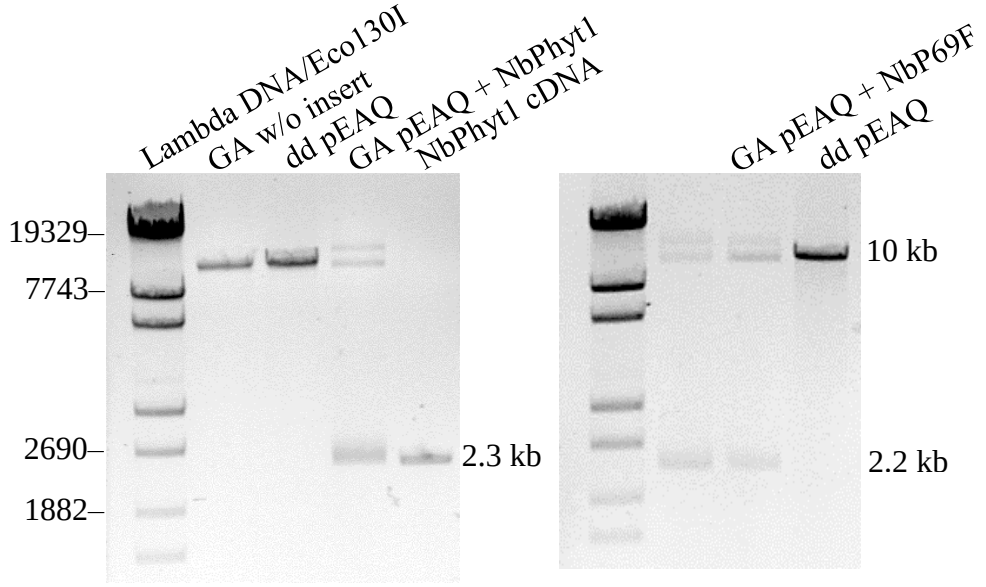

Figure 8. Cloning of NbPhyt1 (left) and NbP69F (right) cDNA into dd pEAQ

Figure 8 shows distinct bands corresponding to dd pEAQ (~10 kb), NbPhyt1/NbP69F cDNA insert (~2.3/2.2 kb) and the GA product pEAQ-NbPhyt1/NbP69F.

Electrocompetent DH10β *E. coli* were transformed with GA pEAQ-NbPhyt1/NbP69F. 10 colonies were analyzed by colony PCR. The NbPhyt1 DNA sequence was amplified using pEAQ-Fw + NbPhyt1-IntRv primers, with the expected fragment size of ~1.9 kb. The NbP69F DNA sequence was amplified using pEAQ-Rv and NbP69F-IntFw primers, with the expected fragment size of ~1.8 kb.

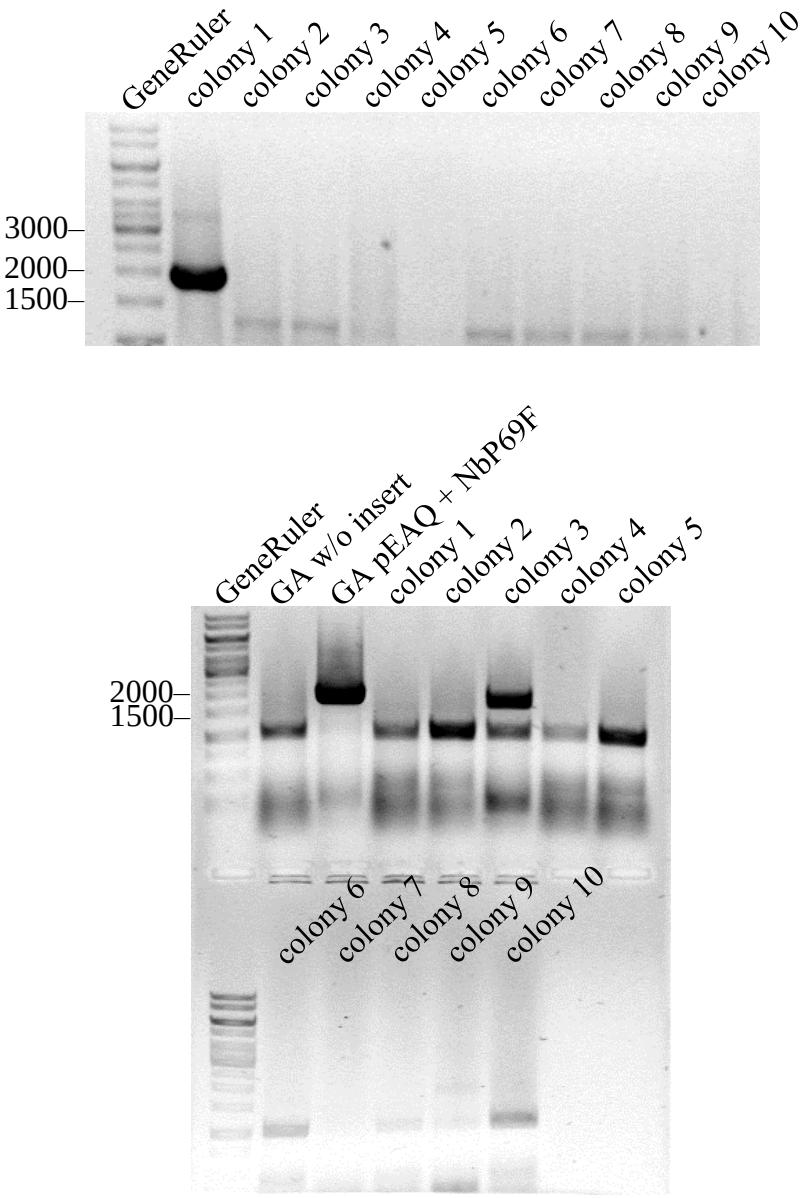

Figure 9. Colony PCR; testing for pEAQ-NbPhyt1 (up) and pEAQ-NbP69F (down) positive colonies

One pEAQ-NbPhyt1 (Figure 9, up) and two pEAQ-NbP69F (Figure 9, down) positive clones were detected, termed colony (col) 1 and col3/9, respectively. These were further propagated for plasmid isolation. Restriction analysis of the isolated col1 plasmid was performed with *Bam*HI – the expected fragments for pEAQ-NbPhyt1 are 9851, 1383 and 1022 bp in size. Restriction

analysis of the isolated col3 and col9 plasmids was performed with *Pst*I – the expected fragments for pEAQ-NbP69F are 5074, 2511, 2381, 1573, 363 and 276 bp in size.

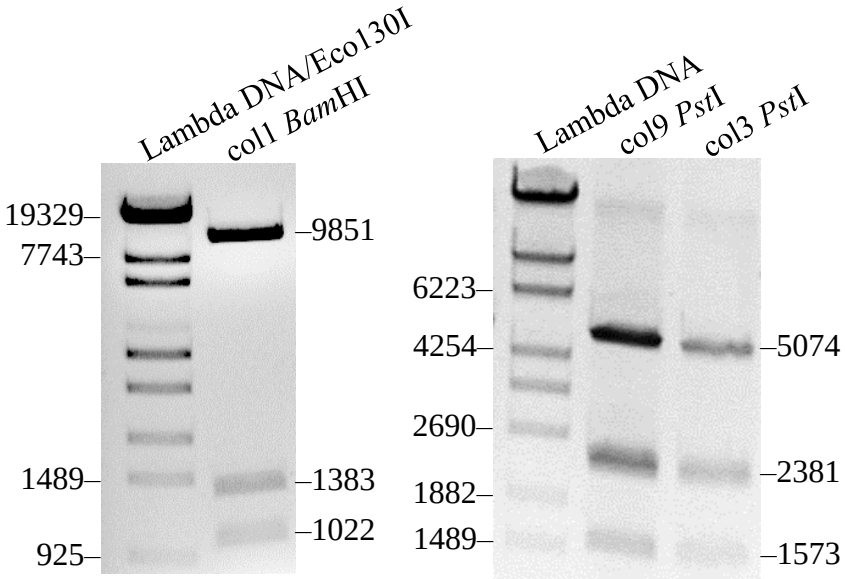

Figure 10. *Bam*HI restriction analysis of col1 isolated plasmid (left) and *Pst*I restriction analysis of col3 and col9 isolated plasmids (right).

Figure 10 shows bands corresponding to the abovementioned fragment sizes, indicating that the isolated plasmids are indeed pEAQ-NbPhyt1 and pEAQ-NbP69F. In the latter case, not all fragments are visible on the gel, however those bands that are detectable correspond to expected restriction fragments of pEAQ-NbP69F. NbPhyt1 and NbP69F (col9) cDNA sequences were confirmed by Sanger sequencing.

A. tumefaciens UIA143 was transformed with pEAQ-NbPhyt1/NbP69F via electroporation. Bacteria were plated, grown and propagated preparing for agroinfiltration.

4.2. EXPRESSION AND PURIFICATION OF RECOMBINANT SUBTILASES

Leaf infiltration of 5-week-old *N. benthamiana* plants was performed with transformed agrobacteria. Apoplastic fluid was collected three days post-infiltration and recombinant his-tagged proteins were isolated/purified by affinity chromatography.

4.2.1. Isolation and purification of NbPhyt1 and NbP69F

1 mL wash and elution fractions were collected. Their absorbance was measured spectrophotometrically at a wavelength of 280 nm (Figure 11). Washing was stopped when A_{280} reached 0.01 and/or was not changing, followed by collection of elution fractions in the same manner.

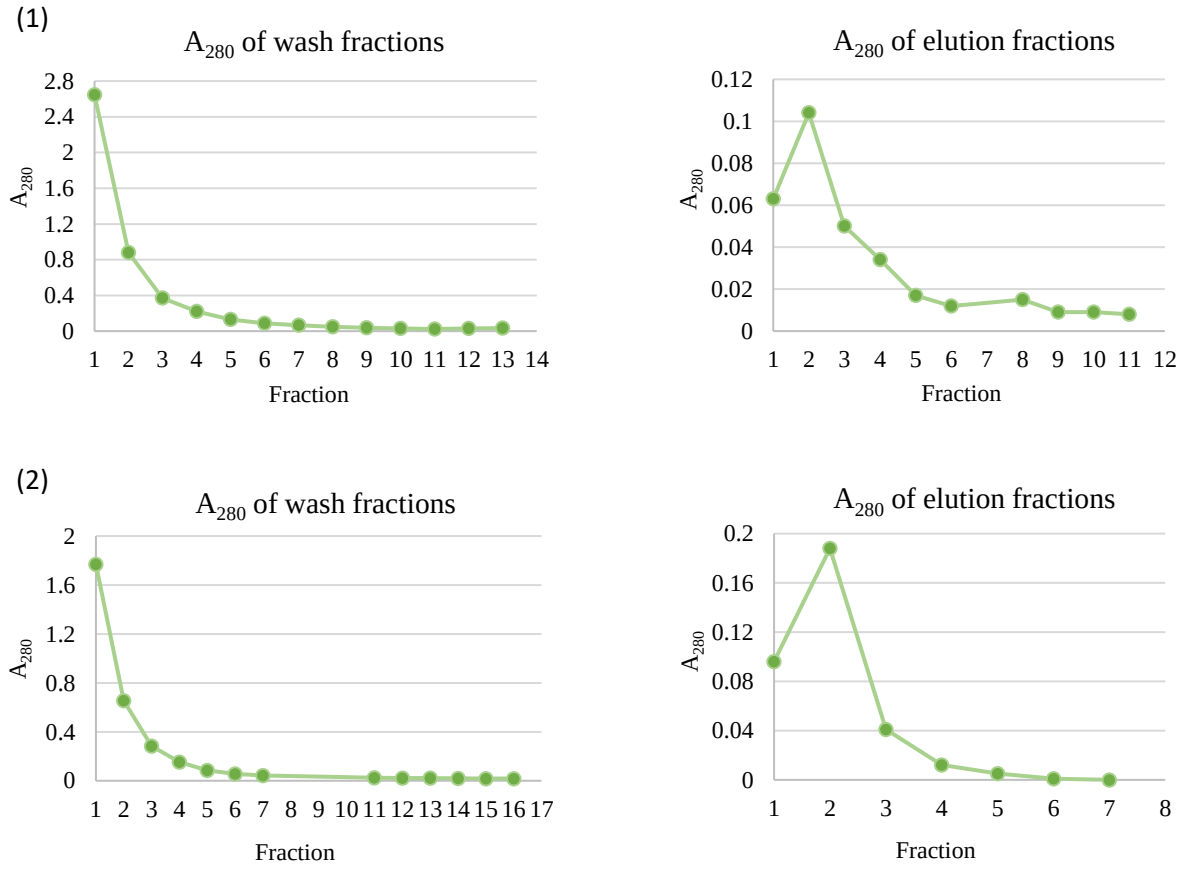

Figure 11. Absorbance at 280 nm of wash and elution fractions acquired during affinity chromatography of the collected apoplastic fluid from NbPhyt1 (1) and NbP69F (2) infiltrated *N. benthamiana* leaves

The spectrophotometric data show an exponential-like decrease in A_{280} values with progression of column washing. The highest A_{280} value of the eluates, indicating the highest protein concentration, is obtained in the second elution fraction. Elution fractions (1) E1-E5 and (2) E1-E4 were pooled and concentrated.

Samples collected throughout the NbPhyt1/NbP69F isolation and purification process – total soluble protein (TSP), apoplastic fluid (AF), flow-through (FT), wash fractions (WX) and concentrated retentate (recombinant NbPhyt1/NbP69F) – were tested for the presence of recombinant NbPhyt1/NbP69F by immunoblotting with α-6xHis and α-SBT1 antibodies. TSP and AF of mock-infiltrated (UIA143 without plasmid) leaves were used as negative controls. Previously collected TSP of UIA143_pEAQ-NbPhyt1 infiltrated leaves was used as a positive control.

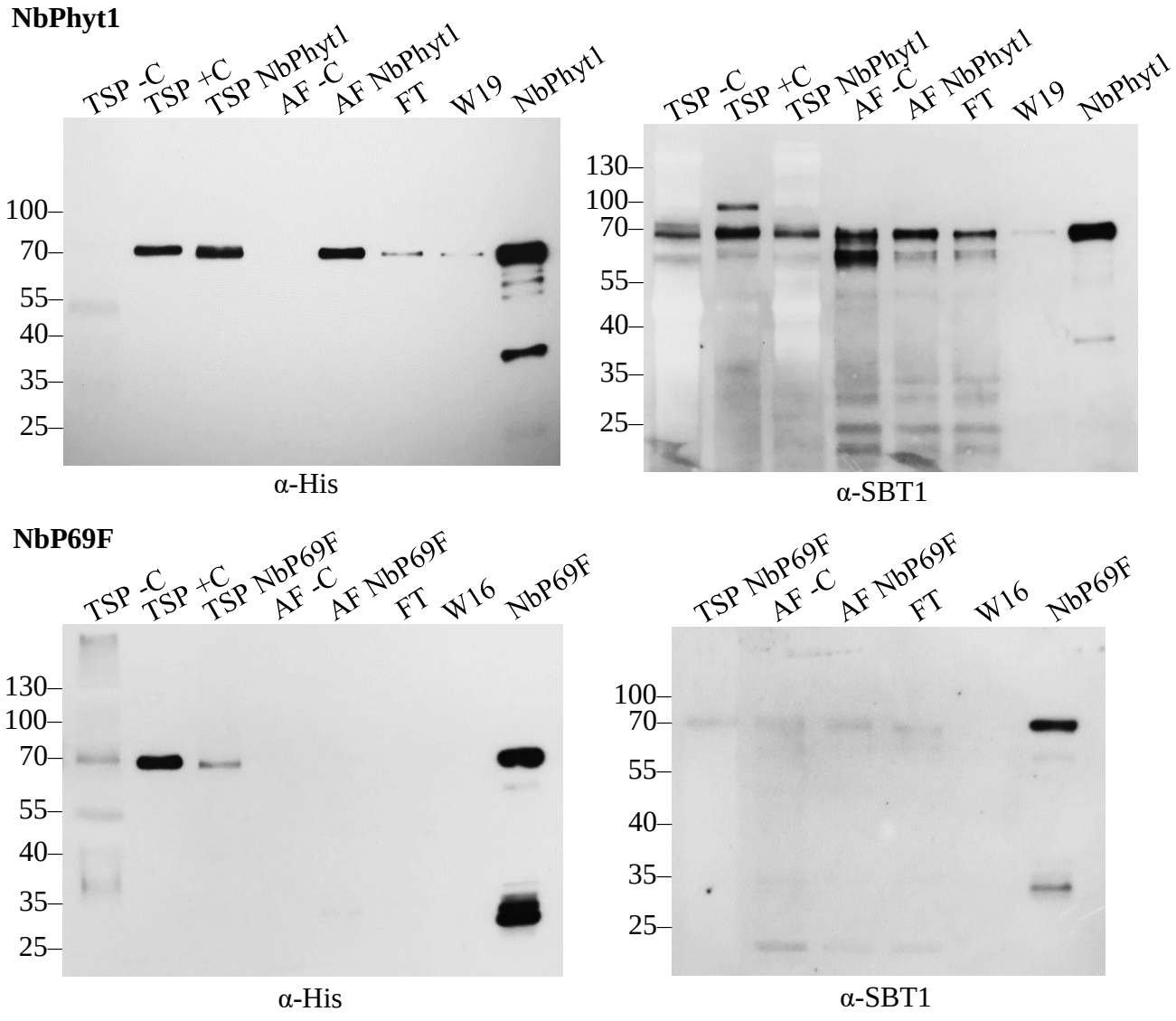

Figure 12. Identification of recombinant NbPhyt1/NbP69F; α-His and α-SBT1 immunoblotting

In both α-His and α-SBT1 blots (Figure 12, up), a 70 kDa band corresponding to the full-sized NbPhyt1 was detected in TSP and AF of UIA143_pEAQ-NbPhyt1 infiltrated leaves, as well as in purified and concentrated NbPhyt1, as expected. The latter also shows multiple bands of smaller sizes indicating NbPhyt1degradation. In this regard, the most intense band is 35-40 kDa in size, especially in the α-His blot. This implies NbPhyt1 is autoreactive (self-processing), however not at its (his-tagged) C-terminus. A weak α-His signal was detected in the flow-through and last wash fraction, indicating that not all of the his-tagged protein bound to the column successfully and that some was also lost during washing. Strong α-SBT1 signals of various sizes were detected in other samples as well, indicating that antibodies against tomato SBT1 cross-react with other *N. benthamiana* proteins, most likely other subtilisin-like Ser peptidases.

In the α-His blot (Figure 12, down left), a 70 kDa band corresponding to the full-sized NbP69F was detected in TSP of UIA143_pEAQ-NbP69F infiltrated leaves, while the AF of UIA143_pEAQ-NbP69F infiltrated leaves showed only very faint bands (not visible here) corresponding to 70 and 25-35 kDa. In both α-His and α-SBT1 blots (Figure 12, down), multiple bands were detected in purified and concentrated NbP69F, corresponding to the full-sized NbP69F (70 kDa) and its degradation products, the most abundant ones being 25-35 kDa in size. This implies NbP69F is autoreactive (self-processing), however not at its (his-tagged) C-terminus. The α-SBT1 blot shows seemingly unspecific bands in the AF negative control, FT and TSP/AF of UIA143_pEAQ-NbP69F infiltrated leaves samples, all displaying a similar staining pattern. This implies, as mentioned above, that antibodies against tomato SBT1 cross-react with other *N. benthamiana* proteins.

4.2.3. Coomassie staining

To evaluate the concentrations of purified NbPhyt1 and NbP69F, proteins were separated by SDS-PAGE and Coomassie Brilliant Blue staining was performed. Concentrations were previously estimated by spectrophotometric measurements at A_{280}.

NbPhyt1 was expressed in *N. benthamiana* leaves, isolated and purified on three separate occasions (NbPhyt1 1º, 2º, 3º) – 15 µL of each purified and concentrated enzyme batch was loaded onto the gel; NbP69F – 5 and 10 µL of purified and concentrated enzyme was loaded onto the gel. NbSBT2 was isolated and purified by Puchol Tarazona (2019) and served as a control sample.

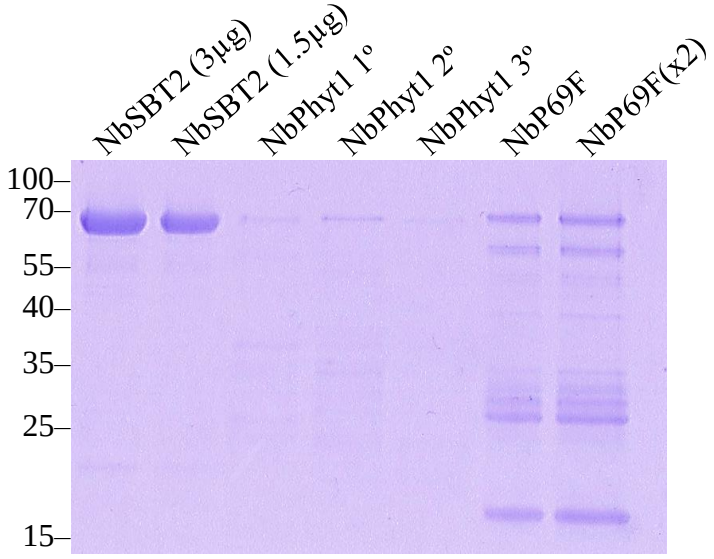

Figure 13. Coomassie Brilliant Blue gel staining: estimation of NbPhyt1/NbP69F concentration

Figure 13 shows a high degree of proteolytic processing of both NbPhyt1 and NbP69F. ~70 kDa fragments corresponding to the full-sized enzymes are visible in all samples. The actual concentration of NbPhyt1 is considerably lower than expected in all three batches, as compared to estimates based on A_{280} measurements (data not shown). On the other hand, NbP69F does not show such discrepancy between the SDS-PAGE and spectrophotometric data.

4.2.2. Activity-based protein profiling

The reactivity of the ABPs FP-biotin and biotinyl-YVAD-CMK with recombinant NbPhyt1/NbP69F was analyzed. NbSBT1 and NbSBT2 labelled with FP-biotin and biotinyl-YVAD-CMK, respectively, were used as positive controls. NbPhyt1/NbP69F samples without added probes were used as negative controls.

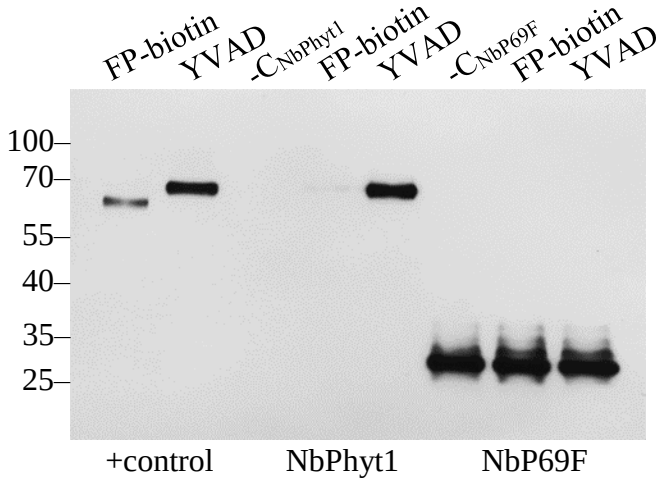

Figure 14. Labelling of recombinant NbPhyt1 and NbP69F with FP-biotin and biotinyl-YVAD-CMK

Figure 14 implies that NbPhyt1 reacts only weakly with FP-biotin, as shown by the faint 70 kDa band. Much like NbSBT2 which selectively cleaves after aspartic acid residues (Puchol Tarazona *et al.*, 2021), NbPhyt1 reacts strongly with biotinyl-YVAD-CMK, as shown by the high-intensity 70 kDa band.

NbP69F-ABP samples show bands similar in size (25-35 kDa) and intensity. 25-35 kDa bands were previously observed in α-His and α-SBT1 blots (Figure 12, down), implying that the NbP69F catalytic subunit is contained within the C-terminal 25-35 kDa fragment. However, similar bands are observed in the NbP69F -control sample (no probe), thus no conclusion can be made about the enzyme's activity towards ABPs. A mistake had possibly been made during preparation of the -C reaction. On the other hand, the unusual signal similarity in all NbP69F samples implies non-specific reactivity of streptavidin-HRP with the enzyme.

4.3. ACTIVITY OF RECOMBINANT SUBTILASES TOWARDS mAbs

4.3.1. *In vitro* antibody degradation assays

MAbs PG9, 2F5, 2G12-wt and 2G12-I19R were tested for their susceptibility to proteolytic degradation by NbPhyt1 (Figure 15) and NbP69F (Figure 16), at pH 5.5. Aliquots for analysis were taken at t = 0, 30 minutes, 2 hours, 4.5 hours and overnight. Control samples, taken at t = 0 and overnight, didn't contain the respective enzyme.

NbPhyt1:

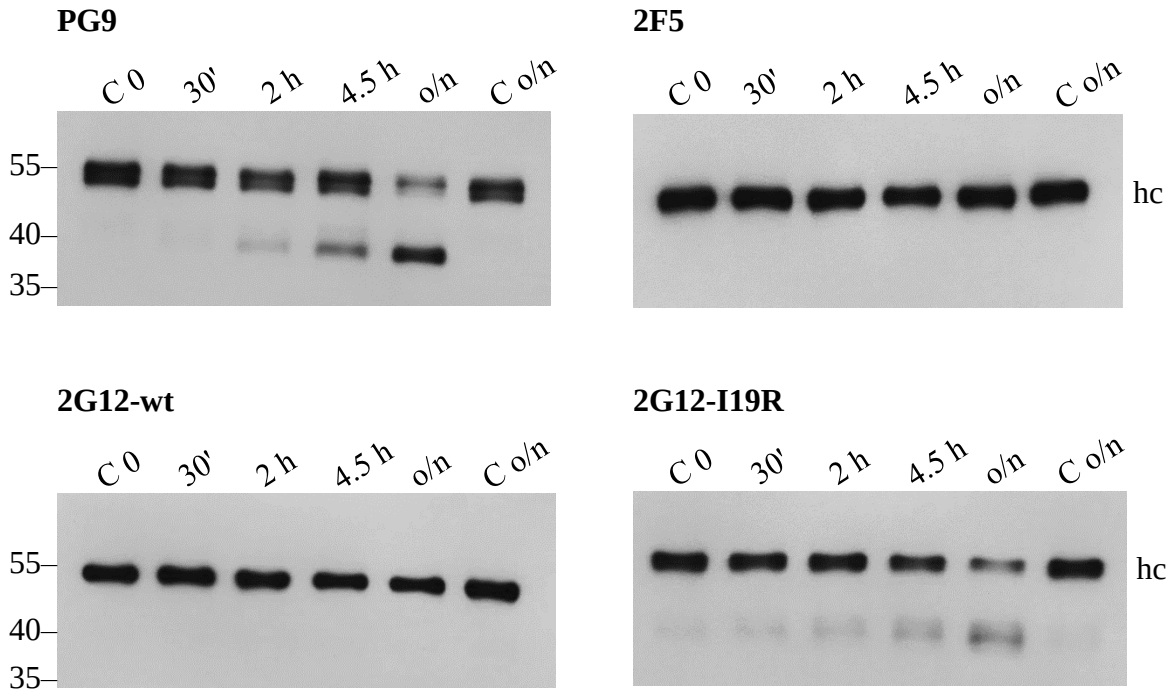

Figure 15. *In vitro* proteolytic degradation of PG9, 2F5, 2G12-wt and 2G12-I19R by NbPhyt1

PG9 digest with recombinant NbPhyt1 is observed – the intensity of the band corresponding to the characteristic 40 kDa PG9 heavy chain degradation product increases over time. Degradation products of the same size have been observed previously during PG9 production in *N. benthamiana* leaves (Niemer *et al.*, 2014) and recently two *N. benthamiana* peptidases, NbSBT1 and NbSBT2, have been identified to cleave PG9 *in vitro* (Puchol Tarazona *et al.*, 2021).

It has been demonstrated previously that 2F5 is susceptible to processing upon incubation with leaf apoplastic fluid and total soluble protein leaf extract, the cleavage occurring at the tip of the

22-residue long, sterically exposed CDRH3 loop (Niemer *et al.*, 2014). However, the Ab appears to be resistant to NbPhyt1 activity, which was also observed with the recently characterized NbSBT2 (Puchol Tarazona *et al.*, 2021).

NbPhyt1 shows no reactivity towards 2G12-wt. The Ab's invulnerability to proteolysis is also observed upon incubation with apoplastic fluid (Niemer *et al.*, 2014), most likely due to its domain-swapped structure that restricts access to its CDRH3s, as well as shorter CDRH3s (14 residues). Conversely, the nondomain-exchanged variant 2G12-I19R is susceptible to proteolytic cleavage (Puchol Tarazona *et al.*, 2020), which is in accordance with the results presented here – 2G12-I19R cleavage with NbPhyt1 yields a 40 kDa heavy-chain degradation product, which increases over time.

NbP69F:

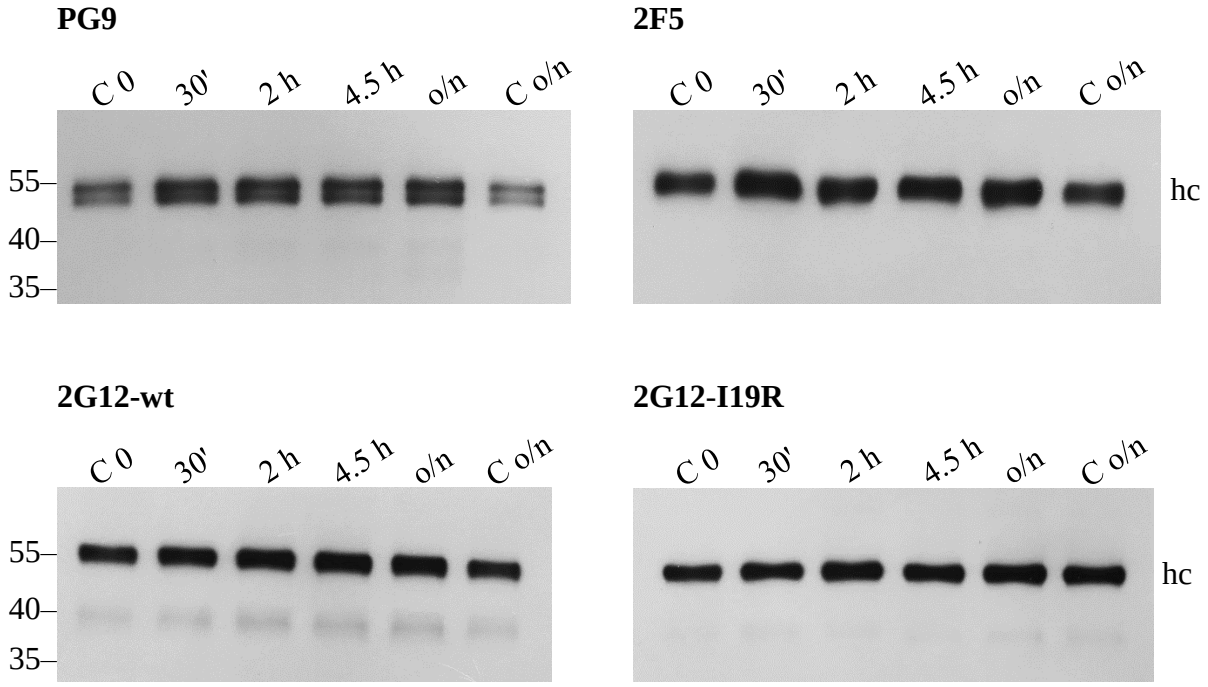

Figure 16. *In vitro* proteolytic degradation of PG9, 2F5, 2G12-wt and 2G12-I19R by NbP69F

No Ab digest is observed with recombinant NbP69F, indicating no reactivity towards PG9, 2F5, 2G12-wt and 2G12-I19R mAbs under the tested conditions. Other possible explanations of the apparent inactivity of purified NbP69F are rapid self-digestion (indicated by the abundance of 25-

35 kDa fragments, as shown above) and/or loss of activity due to suboptimal storage conditions, e.g. multiple freeze-thaw cycles. The latter were shown to significantly reduce the proteolytic activity of NbPhyt1 towards PG9 (data not shown).

4.3.2. NbPhyt1 inhibitor profiling

The proteolytic activity of NbPhyt1 towards PG9 and 2G12-I19R was also tested after pre-treatment with the following inhibitors: AEBSF(20 mM, 1mM), PMSF (1 mM), FP-biotin (100 µM), Ac-YVAD-CMK (100 µM), Z-VAD-FMK (100 µM). The negative control sample (t = 0, o/n) contained final buffer instead of enzyme. The positive control sample contained 1% DMSO instead of inhibitor.

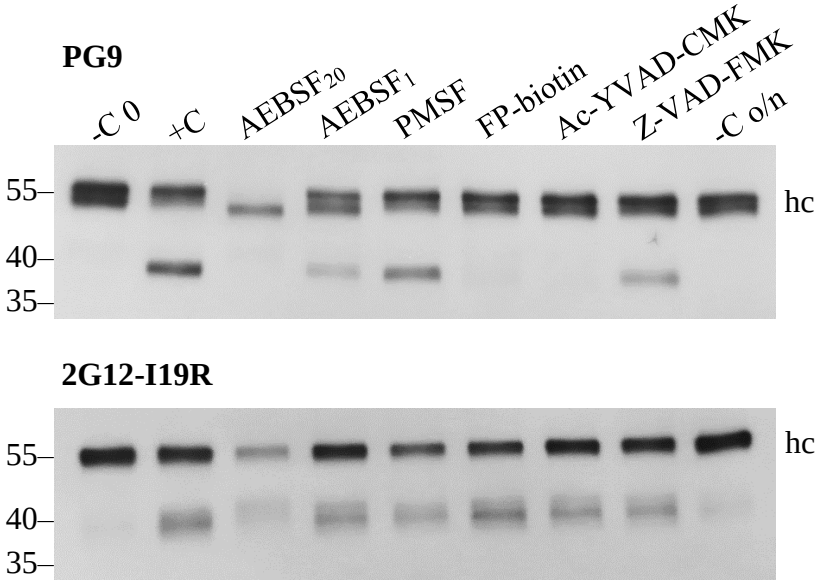

Figure 17. Effect of protease inhibitors on *in vitro* proteolytic degradation of PG9 (up) and 2G12-I19R (down) by NbPhyt1

Figure 17 shows bands corresponding to the full-length PG9/2G12-I19R 55 kDa heavy chain and its 40 kDa degradation product. Of all tested inhibitors, the strongest and seemingly complete inhibition of NbPhyt1 proteolytic activity towards PG9 is observed with FP-biotin and Ac-YVAD-CMK. In the ABPP experiment (Figure 14), FP-biotin did not react strongly with NbPhyt1. The higher concentration (100 µM) of the inhibitor used in this experiment compared to the active site

labelling (1 µM) could account for the strong reactivity of NbPhyt1 with FP-biotin. Next in the inhibitory strength is AEBSF (1 mM), followed by Z-VAD-FMK. Higher concentrations of AEBSF (20 mM) seem to precipitate the Ab, hence no conclusions on the inhibitory activity can be made. Lastly, fairly weak but still observable inhibition can be seen with PMSF. It was previously noted that processing of PG9 with *N. benthamiana* apoplastic fluid is most efficiently inhibited by a combination of AEBSF and (Ac)-YVAD-CMK (Puchol Tarazona *et al.*, 2020).
2G12-I19R shows a similar degradation pattern in all samples, implying that proteolytic degradation of the Ab is not inhibited by any of the tested inhibitors, which was not expected. Therefore, it is inconclusive whether the 2G12-I19R digest is a result of NbPhyt1 activity. Again, 20 mM AEBSF seems to precipitate the Ab.

4.3.3. NbPhyt1 pH profiling

The NbPhyt1 activity towards CHO-PG9 was tested at various pH values. The pH was adjusted with appropriate McIlvaine buffers (Table 6). The negative control sample contained final buffer instead of enzyme and 1xPBS instead of McIlvaine buffer.

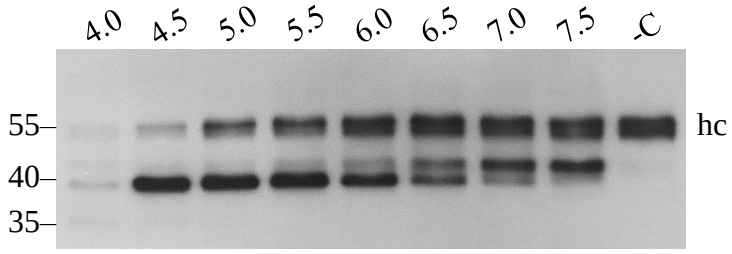

Figure 18. NbPhyt1 activity towards PG9 at pH 4.0-7.5

Figure 18 shows that NbPhyt1 is reactive towards PG9 at all tested pH values. Judging from the intensity of the 55 and 40 kDa bands corresponding to the PG9 heavy chain and its degradation products, respectively, recombinant NbPhyt1 is most reactive towards the Ab between pH 4.0 and 5.5. This is in accordance with the enzyme's activity in the apoplastic fluid (pH~5.5), as well as the recently determined 4.0-4.5 pH optima of PG9 hydrolysis by apoplastic proteases (Puchol Tarazona *et al.*, 2020). At pH 4.0 multiple faint bands are visible, suggesting unspecific degradation. The low intensity of the bands implies that PG9 is unstable under such conditions and

possibly more accessible to the peptidase. Similar Ab degradation at low pH values was observed previously with *N. tabacum* leaf extract (Hehle *et al.*, 2011). Furthermore, it was suggested that the Fc region of IgG molecules is partially denatured at low pH values, thus making Abs more susceptible to degradation (Kim et al., 1995). Degradation of PG9 is strong but mostly unchanged at pH ≥ 6.0. Two bands of about 40 kDa are present in all NbPhyt1 treated samples. This is likely due to differences in Tyr sulfation of the Ab (4.3.4). Upon cleavage, the sulfated tyrosine is possibly more exposed to its environment; the sulfate ester is acid labile and hydrolyses to tyrosine in acidic conditions (Balsved *et al.*, 2007) – the unsulfated heavy chain migrates faster through the gel as discussed below (4.3.4), hence the pH-dependent change in the intensity of the two 40 kDa bands. Alternatively, it is possible that NbPhyt1 additionally cleaves the PG9 heavy chain at a position further upstream at pH ≥ 6.5.

4.3.4. PG9 cleavage site analysis

CHO-PG9 (~250 µg) was digested with recombinant NbPhyt1. The Ab was purified from the reaction mixture by protein A affinity chromatography and the buffer was exchanged to PBS. The efficiency of the Ab digest was checked by Coomassie Brilliant Blue gel staining (Figure 19). Undigested PG9 served as a negative control. 3 and 6 µg of the Ab were loaded onto the gel. The PG9 cleavage site was identified by LC/MS performed by Daniel Maresch of the Department of Chemistry, BOKU Vienna.

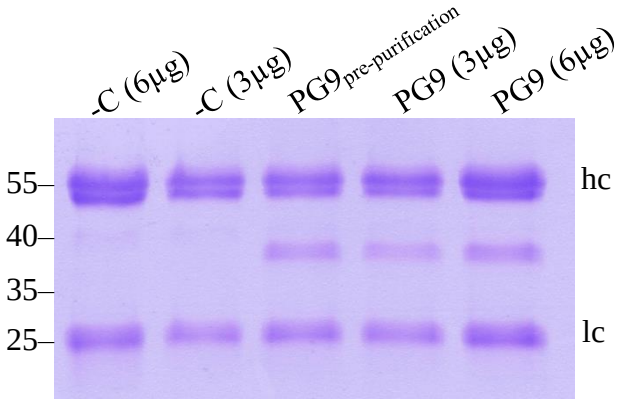

Figure 19. PG9 digestion by NbPhyt1

Figure 19 shows the extent of PG9 digestion by NbPhyt1 after incubation for 1.5 days. The distinct bands observed here correspond to the 55 kDa Ab heavy chain, the 40 kDa heavy chain degradation product and the 25 kDa Ab light chain.

MS analysis of undigested PG9 reveals similar amounts of un- and monosulfated heavy chain moieties. The PG9 heavy chain carrying one sulfated tyrosine is 79 Da larger compared to the unsulfated species. The negative charge of the sulfated Tyr could reduce SDS binding to the protein, resulting in slower migration through the electric field and thus explaining the two 55 kDa bands. Different forms of Tyr sulfation, their role in Ab specificity and contribution to neutralization have been reported for PG9 (Pejchal *et al.*, 2010). It has been shown that sulfated PG9 neutralizes HIV-1 with much higher potency than the unsulfated Ab (Loos *et al.*, 2015). Regarding this, the critical sulfo-Tyr residues are located in the antigen-binding site, more specifically the CDRH3.

The primary structure of the PG9 heavy chain is shown below: the CDRH3 loop is highlighted in teal and its tip in grey, with the red arrow indicating the identified cleavage site.

PG9 (heavy chain):

QRLVESGGGVVQPGSSLRLSCAASGFDFSRQGMHWVRQAPGQGLEWV
AFIKYDGSEKYHADSVWGRLSISRDNSKDTLYLQMNSLRVEDTATYFC
VREAGGPDYRNGYNYYD↓FYDGYYNYHYMDVWGKGTTVTVSSASTK
GPSVFPLAPSSKSTSGGTAALGCLVKDYFPEPVTVSWNSGALTSGVHTF
PAVLQSSGLYSLSSVVTVPSSSLGTQTYICNVNHKPSNTKVDKKVEPKS
CDKTHTCPPCPAPELLGGPSVFLFPPKPKDTLMISRTPEVTCVVVDVSHE
DPEVKFNWYVDGVEVHNAKTKPREEQYNSTYRVVSVLTVLHQDWLN
GKEYKCKVSNKALPAPIEKTISKAKGQPREPQVYTLPPSRDELTKNQVS
LTCLVKGFYPSDIAVEWESNGQPENNYKTTPPVLDSDGSFFLYSKLTVD
KSRWQQGNVFSCSVMHEALHNHYTQKSLSLSPGK

NbPhyt1 performs a single cleavage of the PG9 heavy chain at the tip of its CDRH3 loop, at the position NYYD^{112}↓F^{113}YDG. Cleavage immediately after the aspartic acid residue is in accordance with the known specificity of phytaspases (Chichkova *et al.*, 2014; Galiullina *et al.*, 2015; Reichardt *et al.*, 2018). The PG9 CDRH3 loop is exceptionally long (28 residues), thus the cleavage site surface is exposed and sterically accessible. Cleavage at NYYD^{112}↓F^{113}YDG was

found in PG9 expressed in *N. benthamiana* leaves (Niemer *et al.*, 2014), and PG9 incubated *in vitro* with *N. benthamiana* apoplastic fluid (Puchol Tarazona *et al.*, 2020). The recently identified NbSBT2 also cleaves PG9 at this position (Puchol Tarazona *et al.*, 2021). No processing of the PG9 light chain was identified.

5. CONCLUSIONS

According to the results presented in this thesis, the following conclusions can be made:

1. Recombinant subtilases NbPhyt1 and NbP69F were successfully expressed in *Nicotiana benthamiana* leaves and could be isolated from the apoplastic fluid by IMAC affinity chromatography.
2. Purified and concentrated NbPhyt1 and NbP69F undergo progressive proteolytic degradation, likely by autoproteolysis.
3. NbP69F does not cleave PG9, 2F5, 2G12-wt and 2G12-I19R under the tested conditions.
4. NbPhyt1 proteolytically cleaves PG9 *in vitro*, at the tip of its CDRH3 loop after the aspartic acid residue D^{112}. The enzyme does not cleave the Ab light chain.
5. NbPhyt1 activity towards PG9 is pH dependent, with the strongest Ab proteolysis at pH 4.0-5.5.
6. NbPhyt1 activity towards PG9 is strongly inhibited by FP-biotin and Ac-YVAD-CMK, followed by AEBSF and Z-VAD-FMK.
7. NbPhyt1 does not cleave 2F5 and 2G12-wt under the tested conditions.

6. REFERENCES

Abas, A. K., Lichtman, A. H., Pillai, S. (2011) Cellular and molecular immunology, 7th ed., Saunders Elsevier, Philadelphia, pp. 89-107.

Alvarez, M. L., Topal, E., Martin, F., Cardineau, G. A. (2010) Higher accumulation of F1-V fusion recombinant protein in plants after induction of protein body formation. *Plant Mol. Biol.* **72**, 75–89.

Bally, J., Job, C., Belghazi, M., Job, D. (2011) Metabolic adaptation in transplastomic plants massively accumulating recombinant proteins. *PLoS One* **6**.

Bally, J., Jung, H., Mortimer, C., Naim, F., Philips, J. G., Hellens, R., Bombarely, A., Goodin, M. M., Waterhouse, P. M. (2018) The rise and rise of Nicotiana benthamiana: A plant for all reasons. *Annu. Rev. Phytopathol.* **56**, 405–426.

Balsved, D., Bundgaard, J. R., Sen, J. W. (2007) Stability of tyrosine sulfate in acidic solutions. *Anal. Biochem.* **363**, 70–76.

Barbato, G., Bianchi, E., Ingallinella, P., Hurni, W. H., Miller, M. D., Ciliberto, G., Cortese, R., Bazzo, R., Shiver, J. W., Pessi, A. (2003) Structural analysis of the epitope of the anti-HIV antibody 2F5 sheds light into its mechanism of neutralization and HIV fusion. *J. Mol. Biol.* **330**, 1101–1115.

Benchabane, M., Goulet, C., Rivard, D., Faye, L., Gomord, V., Michaud, D. (2008) Preventing unintended proteolysis in plant protein biofactories. *Plant Biotechnol. J.* **6**, 633–648.

Bennett, C. F., Swayze, E. E. (2010) RNA targeting therapeutics: Molecular mechanisms of antisense oligonucleotides as a therapeutic platform. *Annu. Rev. Pharmacol. Toxicol.* **50**, 259–293.

Blattner, C., Lee, J. H., Sliepen, K., Derking, R., Falkowska, E., la Peña, A. T. de, Cupo, A., Julien, J.-P., Gils, M. van, Lee, P. S., Peng, W., Paulson, J. C., Poignard, P., Burton, D. R., Moore, J. P., Sanders, R. W., Wilson, I. A., Ward, A. B. (2014) Structural delineation of a quaternary, cleavage-dependent epitope at the gp41-gp120 interface on intact HIV-1 env trimers. *Immunity* **40**, 669–680.

Bonsignori, M., Zhou, T., Sheng, Z., Chen, L., Gao, F., Joyce, M. G., Ozorowski, G., Chuang, G.

Y., Schramm, C. A., Wiehe, K., Alam, S. M., Bradley, T., Gladden, M. A., Hwang, K. K., Iyengar, S., Kumar, A., Lu, X., Luo, K., Mangiapani, M. C., Parks, R. J., Song, H., Acharya, P., Bailer, R. T., Cao, A., Druz, A., Georgiev, I. S., Kwon, Y. D., Louder, M. K., Zhang, B., Zheng, A., Hill, B. J., Kong, R., Soto, C., Mullikin, J. C., Douek, D. C., Montefiori, D. C., Moody, M. A., Shaw, G. M., Hahn, B. H., Kelsoe, G., Hraber, P. T., Korber, B. T., Boyd, S. D., Fire, A. Z., Kepler, T. B., Shapiro, L., Ward, A. B., Mascola, J. R., Liao, H. X., Kwong, P. D., Haynes, B. F. (2016) Maturation pathway from germline to broad HIV-1 neutralizer of a CD4-mimic antibody. *Cell* **165**, 449–463.

Bosch, D., Castilho, A., Loos, A., Schots, A., Steinkellner, H. (2013) N-glycosylation of plant-produced recombinant proteins. *Curr. Pharm. Des.* **19**, 5503–5512.

Burnett, M. J. B., Burnett, A. C. (2020) Therapeutic recombinant protein production in plants: Challenges and opportunities. *Plants, People, Planet* **2**, 121–132.

Burton, D. R., Ahmed, R., Barouch, D. H., Butera, S. T., Crotty, S., Godzik, A., Kaufmann, D. E., McElrath, M. J., Nussenzweig, M. C., Pulendran, B., Scanlan, C. N., Schief, W. R., Silvestri, G., Streeck, H., Walker, B. D., Walker, L. M., Ward, A. B., Wilson, I. A., Wyatt, R. (2012) *A blueprint for HIV vaccine discovery*. *Cell Host Microbe* **12**, 396-407.

Burton, D. R., Pyati, J., Koduri, R., Sharp, S. J., Thornton, G. B., Parren, P. W. H. I., Sawyer, L. S. W., Hendry, R. M., Dunlop, N., Nara, P. L., Lamacchia, M., Garratty, E., Stiehm, E. R., Bryson, Y. J., Cao, Y., Moore, J. P., Ho, D. D., Barbas, C. F. (1994) Efficient neutralization of primary isolates of HIV-1 by a recombinant human monoclonal antibody. *Science* **266**, 1024–1027.

Calarese, D. A., Scanlan, C. N., Zwick, M. B., Deechongkit, S., Mimura, Y., Kunert, R., Zhu, P., Wormald, M. R., Stanfield, R. L., Roux, K. H., Kelly, J. W., Rudd, P. M., Dwek, R. A., Katinger, H., Burton, D. R., Wilson, I. A. (2003) Antibody domain exchange is an immunological solution to carbohydrate cluster recognition. *Science (80-.).* **300**, 2065–2071.

Cardoso, R. M. F., Zwick, M. B., Stanfield, R. L., Kunert, R., Binley, J. M., Katinger, H., Burton, D. R., Wilson, I. A. (2005) Broadly neutralizing anti-HIV antibody 4E10 recognizes a helical conformation of a highly conserved fusion-associated motif in gp41. *Immunity* **22**, 163–173.

Cedzich, A., Huttenlocher, F., Kuhn, B. M., Pfannstiel, J., Gabier, L., Stintzi, A., Schaller, A.

(2009) The protease-associated domain and C-terminal extension are required for zymogen processing, sorting within the secretory pathway, and activity of tomato subtilase 3 (SlSBT3). *J. Biol. Chem.* **284**, 14068–14078.

Chen, Q., Davis, K. R. (2016) The potential of plants as a system for the development and production of human biologics. *F1000Research* **5**, F1000 Faculty Rev-912.

Chichkova, N. V., Galiullina, R. A., Beloshistov, R. E., Balakireva, A. V., Vartapetian, A. B. (2014) Phytaspases: Aspartate-specific proteases involved in plant cell death. *Russ. J. Bioorganic Chem.* **40**, 606–611.

Desai, P. N., Shrivastava, N., Padh, H. (2010) Production of heterologous proteins in plants: Strategies for optimal expression. *Biotechnol. Adv.* **28**, 427–435.

Diskin, R., Scheid, J. F., Marcovecchio, P. M., West, A. P., Klein, F., Gao, H., Gnanapragasam, P. N. P., Abadir, A., Seaman, M. S., Nussenzweig, M. C., Bjorkman, P. J. (2011) Increasing the potency and breadth of an HIV antibody by using structure-based rational design. *Science* **334**, 1289–1293.

Doores, K. J., Burton, D. R. (2010) Variable loop glycan dependency of the broad and potent HIV-1-neutralizing antibodies PG9 and PG16. *J. Virol.* **84**, 10510–10521.

Doores, K. J., Fulton, Z., Huber, M., Wilson, I. A., Burton, D. R. (2010) Antibody 2G12 recognizes Di-mannose equivalently in domain- and nondomain-exchanged Forms but Only binds the HIV-1 glycan shield if domain exchanged. *J. Virol.* **84**, 10690–10699.

Doran, P. M. (2006) Foreign protein degradation and instability in plants and plant tissue cultures. *Trends Biotechnol.* **24**, 426–432.

Durfee, T., Nelson, R., Baldwin, S., Plunkett, G., Burland, V., Mau, B., Petrosino, J. F., Qin, X., Muzny, D. M., Ayele, M., Gibbs, R. A., Csörgo, B., Pósfai, G., Weinstock, G. M., Blattner, F. R. (2008) The complete genome sequence of Escherichia coli DH10B: Insights into the biology of a laboratory workhorse. *J. Bacteriol.* **190**, 2597–2606.

Falkowska, E., Le, K. M., Ramos, A., Doores, K. J., Lee, J. H., Blattner, C., Ramirez, A., Derking, R., Gils, M. J. van, Liang, C.-H., Mcbride, R., Bredow, B. von, Shivatare, S. S., Wu, C.-Y., Chan-Hui, P.-Y., Liu, Y., Feizi, T., Zwick, M. B., Koff, W. C., Seaman, M. S., Swiderek, K., Moore, J.

P., Evans, D., Paulson, J. C., Wong, C.-H., Ward, A. B., Wilson, I. A., Sanders, R. W., Burton, D. R. (2014) Broadly neutralizing HIV antibodies define a glycan-dependent epitope on the pre-fusion conformation of the gp41 protein on cleaved Envelope trimers. *Immunity* **40**, 657–668.

Farrand, S. K., O'Morchoe, S. P., McCutchan, J. (1989) Construction of an Agrobacterium tumefaciens C58 recA mutant. *J. Bacteriol.* **171**, 5314–5321.

Fichtner, F., Urrea Castellanos, R., Ülker, B. (2014) Precision genetic modifications: A new era in molecular biology and crop improvement. *Planta* **239**, 921-939.

Fischer, R., Emans, N. (2000) Molecular farming of pharmaceutical proteins. *Transgenic Res.* **9**, 279–299.

Fischer, R., Schillberg, S., Buyel, J., Twyman, R. (2013) Commercial aspects of pharmaceutical protein production in plants. *Curr. Pharm. Des.* **19**, 5471–5477.

Galiullina, R. A., Kasperkiewicz, P., Chichkova, N. V., Szalek, A., Serebryakova, M. V., Poreba, M., Drag, M., Vartapetian, A. B. (2015) Substrate specificity and possible heterologous targets of phytaspase, a plant cell death protease. *J. Biol. Chem.* **290**, 24806–24815.

Gleba, Y., Klimyuk, V., Marillonnet, S. (2005) Magnifection - A new platform for expressing recombinant vaccines in plants. *Vaccine* **23**, 2042–2048.

Goettig, P. (2016) Effects of glycosylation on the enzymatic activity and mechanisms of proteases. *Int. J. Mol. Sci.* **17**, 1969.

Goldsby, R. A., Kindt, T. J., Osborne, B. A., Kuby, J. (2003) Immunology, 5th ed., W.H. Freeman, New York, pp. 76-101.

Göritzer, K., Maresch, D., Altmann, F., Obinger, C., Strasser, R. (2017) Exploring site-specific N-glycosylation of HEK293 and plant-produced Human IgA isotypes. *J. Proteome Res.* **16**, 2560–2570.

Grosse-Holz, F., Kelly, S., Blaskowski, S., Kaschani, F., Kaiser, M., Hoorn, R. A. L. van der (2018) The transcriptome, extracellular proteome and active secretome of agroinfiltrated Nicotiana benthamiana uncover a large, diverse protease repertoire. *Plant Biotechnol. J.* **16**, 1068–1084.

Grosse-Holz, F. M., Hoorn, R. A. L. van der (2016) Juggling jobs: roles and mechanisms of

multifunctional protease inhibitors in plants. *New Phytol.* **210**, 794–807.

Grosse-Holz, F., Madeira, L., Zahid, M. A., Songer, M., Kourelis, J., Fesenko, M., Ninck, S., Kaschani, F., Kaiser, M., Hoorn, R. A. L. van der (2018) Three unrelated protease inhibitors enhance accumulation of pharmaceutical recombinant proteins in Nicotiana benthamiana. *Plant Biotechnol. J.* **16**, 1797–1810.

Guo, H.-S., Fei, J.-F., Xie, Q., Chua, N.-H. (2003) A chemical-regulated inducible RNAi system in plants. *Plant J.* **34**, 383–392.

Hamilton, C. M. (1997) A binary-BAC system for plant transformation with high-molecular-weight DNA. *Gene* **200**, 107–116.

Hehle, V. K., Paul, M. J., Drake, P. M., Ma, J. K. C., Dolleweerd, C. J. van (2011) Antibody degradation in tobacco plants: A predominantly apoplastic process. *BMC Biotechnol.* **11**, 128.

Hellens, R., Mullineaux, P., Klee, H. (2000) A guide to Agrobacterium binary Ti vectors. *Trends Plant Sci.* **5**, 446–451.

Hemelaar, J. (2012) The origin and diversity of the HIV-1 pandemic. *Trends Mol. Med.* **18**, 182–192.

Hoorn, R. A. L. van der (2008) Plant proteases: From phenotypes to molecular mechanisms. *Annu. Rev. Plant Biol.* **59**, 191–223.

Huang, J., Ofek, G., Laub, L., Louder, M. K., Doria-Rose, N. A., Longo, N. S., Imamichi, H., Bailer, R. T., Chakrabarti, B., Sharma, S. K., Alam, S. M., Wang, T., Yang, Y., Zhang, B., Migueles, S. A., Wyatt, R., Haynes, B. F., Kwong, P. D., Mascola, J. R., Connors, M. (2012) Broad and potent neutralization of HIV-1 by a gp41-specific human antibody. *Nature* **491**, 406–412.

James, E. A., Wang, C., Wang, Z., Reeves, R., Shin, J. H., Magnuson, N. S., Lee, J. M. (2000) Production and characterization of biologically active human GM-CSF secreted by genetically modified plant cells. *Protein Expr. Purif.* **19**, 131–138.

Julien, J.-P., Sok, D., Khayat, R., Lee, J. H., Doores, K. J., Walker, L. M., Ramos, A., Diwanji, D. C., Pejchal, R., Cupo, A., Katpally, U., Depetris, R. S., Stanfield, R. L., McBride, R., Marozsan, A. J., Paulson, J. C., Sanders, R. W., Moore, J. P., Burton, D. R., Poignard, P., Ward, A. B., Wilson,

I. A. (2013) Broadly neutralizing antibody PGT121 allosterically modulates CD4 binding via recognition of the HIV-1 gp120 V3 base and multiple surrounding glycans. *PLoS Pathog.* **9**, e1003342.

Kim, N.-S., Kim, T.-G., Kim, O.-H., Ko, E.-M., Jang, Y.-S., Jung, E.-S., Kwon, T.-H., Yang, M.-S. (2008) Improvement of recombinant hGM-CSF production by suppression of cysteine proteinase gene expression using RNA interference in a transgenic rice culture. *Plant Mol. Biol.* **68**, 263–275.

Komarnytsky, S., Borisjuk, N., Yakoby, N., Garvey, A., Raskin, I. (2006) Cosecretion of protease inhibitor stabilizes antibodies produced by plant roots. *Plant Physiol.* **141**, 1185–1193.

Kwon, K.-C., Daniell, H. (2015) Low-cost oral delivery of protein drugs bioencapsulated in plant cells. *Plant Biotechnol. J.* **13**, 1017–1022.

Kwon, T. H., Seo, J. E., Kim, J., Lee, J. H., Jang, Y. S., Yang, M. S. (2003) Expression and secretion of the heterodimeric protein interleukin-12 in plant cell suspension culture. *Biotechnol. Bioeng.* **81**, 870–875.

Kwong, P. D., Mascola, J. R. (2012) Human Antibodies that Neutralize HIV-1: Identification, Structures, and B Cell Ontogenies. *Immunity* **37**, 412–425.

Liao, H. X., Lynch, R., Zhou, T., Gao, F., Munir Alam, S., Boyd, S. D., Fire, A. Z., Roskin, K. M., Schramm, C. A., Zhang, Z., Zhu, J., Shapiro, L., Mullikin, J. C., Gnanakaran, S., Hraber, P., Wiehe, K., Kelsoe, G., Yang, G., Xia, S. M., Montefiori, D. C., Parks, R., Lloyd, K. E., Scearce, R. M., Soderberg, K. A., Cohen, M., Kamanga, G., Louder, M. K., Tran, L. M., Chen, Y., Cai, F., Chen, S., Moquin, S., Du, X., Gordon Joyce, M., Srivatsan, S., Zhang, B., Zheng, A., Shaw, G. M., Hahn, B. H., Kepler, T. B., Korber, B. T. M., Kwong, P. D., Mascola, J. R., Haynes, B. F. (2013) Co-evolution of a broadly neutralizing HIV-1 antibody and founder virus. *Nature* **496**, 469–476.

Lipman, N. S., Jackson, L. R., Trudel, L. J., Weis-Garcia, F. (2005) Monoclonal versus polyclonal antibodies: Distinguishing characteristics, applications, and information resources. *ILAR J.* **46**, 258–267.

Liu, L., Cimbro, R., Lusso, P., Berger, E. A. (2011) Intraprotomer masking of third variable loop (V3) epitopes by the first and second variable loops (V1V2) within the native HIV-1 envelope

glycoprotein trimer. *Proc. Natl. Acad. Sci. U. S. A.* **108**, 20148–20153.

Loos, A., Gach, J. S., Hackl, T., Maresch, D., Henkel, T., Porodko, A., Bui-Minh, D., Sommeregger, W., Wozniak-Knopp, G., Forthal, D. N., Altmann, F., Steinkellner, H., Mach, L. (2015) Glycan modulation and sulfoengineering of anti-HIV-1 monoclonal antibody PG9 in plants. *Proc. Natl. Acad. Sci. U. S. A.* **112**, 12675–12680.

Loos, A., Steinkellner, H. (2014) Plant glyco-biotechnology on the way to synthetic biology. *Front. Plant Sci.* **5**, 523.

López-Otín, C., Bond, J. S. (2008) Proteases: Multifunctional enzymes in life and disease. *J. Biol. Chem.* **283**, 30433–30437.

Ma, J. K. C., Drake, P. M. W., Christou, P. (2003) The production of recombinant pharmaceutical proteins in plants. *Nat. Rev. Genet.* **4**, 794–805.

Ma, L., Lukasik, E., Gawehns, F., Takken, F. L. W. (2012) The use of agroinfiltration for transient expression of plant resistance and fungal effector proteins in nicotiana benthamiana leaves. *Methods Mol. Biol.* **835**, 61–74.

Mandal, M. K., Ahvari, H., Schillberg, S., Schiermeyer, A. (2016) Tackling unwanted proteolysis in plant production hosts used for molecular farming. *Front. Plant Sci.* **7**, 267.

Mandal, M. K., Fischer, R., Schillberg, S., Schiermeyer, A. (2014) Inhibition of protease activity by antisense RNA improves recombinant protein production in Nicotiana tabacum cv. Bright Yellow 2 (BY-2) suspension cells. *Biotechnol. J.* **9**, 1065–1073.

Mao, Y., Wang, L., Gu, C., Herschhorn, A., Xiang, S. H., Haim, H., Yang, X., Sodroski, J. (2012) Subunit organization of the membrane-bound HIV-1 envelope glycoprotein trimer. *Nat. Struct. Mol. Biol.* **19**, 893–899.

McLellan, J. S., Pancera, M., Carrico, C., Gorman, J., Julien, J. P., Khayat, R., Louder, R., Pejchal, R., Sastry, M., Dai, K., O'Dell, S., Patel, N., Shahzad-Ul-Hussan, S., Yang, Y., Zhang, B., Zhou, T., Zhu, J., Boyington, J. C., Chuang, G. Y., Diwanji, D., Georgiev, I., Kwon, Y. Do, Lee, D., Louder, M. K., Moquin, S., Schmidt, S. D., Yang, Z. Y., Bonsignori, M., Crump, J. A., Kapiga, S. H., Sam, N. E., Haynes, B. F., Burton, D. R., Koff, W. C., Walker, L. M., Phogat, S., Wyatt, R., Orwenyo, J., Wang, L. X., Arthos, J., Bewley, C. A., Mascola, J. R., Nabel, G. J., Schief, W. R.,

Ward, A. B., Wilson, I. A., Kwong, P. D. (2011) Structure of HIV-1 gp120 V1/V2 domain with broadly neutralizing antibody PG9. *Nature* **480**, 336–343.

Morimoto, K., Hoorn, R. A. L. van der (2016) The increasing impact of activity-based protein profiling in plant science. *Plant Cell Physiol.* **57**, 446–461.

Mouquet, H., Scharf, L., Euler, Z., Liu, Y., Eden, C., Scheid, J. F., Halper-Stromberg, A., Gnanapragasam, P. N. P., Spencer, D. I. R., Seaman, M. S., Schuitemaker, H., Feizi, T., Nussenzweig, M. C., Bjorkman, P. J. (2012) Complex-type N-glycan recognition by potent broadly neutralizing HIV antibodies. *Proc. Natl. Acad. Sci. U. S. A.* **109**, E3268-E3277.

Niemer, M., Mehofer, U., Torres Acosta, J. A., Verdianz, M., Henkel, T., Loos, A., Strasser, R., Maresch, D., Rademacher, T., Steinkellner, H., Mach, L. (2014) The human anti-HIV antibodies 2F5, 2G12, and PG9 differ in their susceptibility to proteolytic degradation: Down-regulation of endogenous serine and cysteine proteinase activities could improve antibody production in plant-based expression platforms. *Biotechnol. J.* **9**, 493–500.

Ottmann, C., Rose, R., Huttenlocher, F., Cedzich, A., Hauske, P., Kaiser, M., Huber, R., Schaller, A. (2009) Structural basis for Ca2+-independence and activation by homodimerization of tomato subtilase 3. *Proc. Natl. Acad. Sci. U. S. A.* **106**, 17223–17228.

Pancera, M., Zhou, T., Druz, A., Georgiev, I. S., Soto, C., Gorman, J., Huang, J., Acharya, P., Chuang, G. Y., Ofek, G., Stewart-Jones, G. B. E., Stuckey, J., Bailer, R. T., Joyce, M. G., Louder, M. K., Tumba, N., Yang, Y., Zhang, B., Cohen, M. S., Haynes, B. F., Mascola, J. R., Morris, L., Munro, J. B., Blanchard, S. C., Mothes, W., Connors, M., Kwong, P. D. (2014) Structure and immune recognition of trimeric pre-fusion HIV-1 Env. *Nature* **514**, 455–461.

Pantophlet, R., Burton, D. R. (2006) GP120: Target for neutralizing HIV-1 antibodies. *Annu. Rev. Immunol.* **24**, 739–769.

Pejchal, R., Walker, L. M., Stanfield, R. L., Phogat, S. K., Koff, W. C., Poignard, P., Burton, D. R., Wilson, I. A. (2010) Structure and function of broadly reactive antibody PG16 reveal an H3 subdomain that mediates potent neutralization of HIV-1. *Proc. Natl. Acad. Sci. U. S. A.* **107**, 11483–11488.

Peyret, H., Lomonossoff, G. P. (2013) The pEAQ vector series: The easy and quick way to produce

recombinant proteins in plants. *Plant Mol. Biol.* **83**, 51–58.

Powell, J. D. (2015) From pandemic preparedness to biofuel production: Tobacco finds its biotechnology niche in North America. *Agriculture* **5**, 901–917.

Puchol Tarazona, A. A., Lobner, E., Taubenschmid, Y., Paireder, M., Torres Acosta, J. A., Göritzer, K., Steinkellner, H., Mach, L. (2020) Steric accessibility of the cleavage sites dictates the proteolytic vulnerability of the anti-HIV-1 antibodies 2F5, 2G12, and PG9 in plants. *Biotechnol. J.* **15**, e1900308.

Puchol Tarazona, A. A., Maresch, D., Grill, A., Bakalarz, J., Torres Acosta, J. A., Castilho, A., Steinkellner, H., Mach, L. (2021) Identification of two subtilisin-like serine proteases engaged in the degradation of recombinant proteins in Nicotiana benthamiana. *FEBS Lett.* **595**, 379–388.

Qiu, X., Wong, G., Audet, J., Bello, A., Fernando, L., Alimonti, J. B., Fausther-Bovendo, H., Wei, H., Aviles, J., Hiatt, E., Johnson, A., Morton, J., Swope, K., Bohorov, O., Bohorova, N., Goodman, C., Kim, D., Pauly, M. H., Velasco, J., Pettitt, J., Olinger, G. G., Whaley, K., Xu, B., Strong, J. E., Zeitlin, L., Kobinger, G. P. (2014) Reversion of advanced Ebola virus disease in nonhuman primates with ZMapp. *Nature* **514**, 47–53.

Rawlings, N. D., Barrett, A. J., Thomas, P. D., Huang, X., Bateman, A., Finn, R. D. (2018) The MEROPS database of proteolytic enzymes, their substrates and inhibitors in 2017 and a comparison with peptidases in the PANTHER database. *Nucleic Acids Res.* **46**, D624–D632.

Reavy, B., Bagirova, S., Chichkova, N. V., Fedoseeva, S. V., Kim, S. H., Vartapetian, A. B., Taliansky, M. E. (2007) Caspase-resistant VirD2 protein provides enhanced gene delivery and expression in plants. *Plant Cell Rep.* **26**, 1215–1219.

Reichardt, S., Repper, D., Tuzhikov, A. I., Galiullina, R. A., Planas-Marquès, M., Chichkova, N. V., Vartapetian, A. B., Stintzi, A., Schaller, A. (2018) The tomato subtilase family includes several cell death-related proteinases with caspase specificity. *Sci. Rep.* **8**, 10531.

Rivard, D., Anguenot, R., Brunelle, F., Le, V. Q., Vézina, L. P., Trépanier, S., Michaud, D. (2006) An in-built proteinase inhibitor system for the protection of recombinant proteins recovered from transgenic plants. *Plant Biotechnol. J.* **4**, 359–368.

Robert, S., Khalf, M., Goulet, M. C., D'Aoust, M. A., Sainsbury, F., Michaud, D. (2013) Protection

of recombinant mammalian antibodies from development-dependent proteolysis in leaves of Nicotiana benthamiana. *PLoS One* **8**, e70203.

Rozov, S. M., Deineko, E. V. (2019) Strategies for optimizing recombinant protein synthesis in plant cells: classical approaches and new directions. *Mol. Biol.* **53**, 157–175.

Ruf, S., Karcher, D., Bock, R. (2007) Determining the transgene containment level provided by chloroplast transformation. *Proc. Natl. Acad. Sci. U. S. A.* **104**, 6998–7002.

Sainsbury, F., Thuenemann, E. C., Lomonossoff, G. P. (2009) pEAQ: Versatile expression vectors for easy and quick transient expression of heterologous proteins in plants. *Plant Biotechnol. J.* **7**, 682–693.

Salzwedel, K., West, J. T., Hunter, E. (1999) A conserved tryptophan-rich motif in the membrane-proximal region of the human immunodeficiency virus type 1 gp41 ectodomain is important for Env-mediated fusion and virus infectivity. *J. Virol.* **73**, 2469–2480.

Schaller, A. (2004) A cut above the rest: The regulatory function of plant proteases. *Planta* **220**, 183–197.

Schaller, A., Stintzi, A., Rivas, S., Serrano, I., Chichkova, N. V., Vartapetian, A. B., Martínez, D., Guiamét, J. J., Sueldo, D. J., Hoorn, R. A. L. van der, Ramírez, V., Vera, P. (2018) From structure to function – a family portrait of plant subtilases. *New Phytol.* **218**, 901–915.

Scharf, L., Scheid, J. F., Lee, J. H., West, A. P., Chen, C., Gao, H., Gnanapragasam, P. N. P., Mares, R., Seaman, M. S., Ward, A. B., Nussenzweig, M. C., Bjorkman, P. J. (2014) Antibody 8ANC195 reveals a site of broad vulnerability on the HIV-1 envelope spike. *Cell Rep.* **7**, 785–795.

Scheid, J. F., Mouquet, H., Feldhahn, N., Walker, B. D., Pereyra, F., Cutrell, E., Seaman, M. S., Mascola, J. R., Wyatt, R. T., Wardemann, H., Nussenzweig, M. C. (2009) A method for identification of HIV gp140 binding memory B cells in human blood. *J. Immunol. Methods* **343**, 65–67.

Schillberg, S., Raven, N., Spiegel, H., Rasche, S., Buntru, M. (2019) Critical analysis of the commercial potential of plants for the production of recombinant proteins. *Front. Plant Sci.* **10**, 720.

Sharp, J. M., Doran, P. M. (2001) Strategies for enhancing monoclonal antibody accumulation in plant cell and organ cultures. *Biotechnol. Prog.* **17**, 979–992.

Simek, M. D., Rida, W., Priddy, F. H., Pung, P., Carrow, E., Laufer, D. S., Lehrman, J. K., Boaz, M., Tarragona-Fiol, T., Miiro, G., Birungi, J., Pozniak, A., McPhee, D. A., Manigart, O., Karita, E., Inwoley, A., Jaoko, W., DeHovitz, J., Bekker, L.-G., Pitisuttithum, P., Paris, R., Walker, L. M., Poignard, P., Wrin, T., Fast, P. E., Burton, D. R., Koff, W. C. (2009) Human immunodeficiency virus type 1 elite neutralizers: Individuals with broad and potent neutralizing activity identified by using a high-throughput neutralization assay together with an analytical selection algorithm. *J. Virol.* **83**, 7337–7348.

Sontheimer, E. J. (2005) Assembly and function of RNA silencing complexes. *Nat. Rev. Mol. Cell Biol.* **6**, 127–138.

Stoger, E., Fischer, R., Moloney, M., Ma, J. K. C. (2014) Plant molecular pharming for the treatment of chronic and infectious diseases. *Annu. Rev. Plant Biol.* **65**, 743–768.

Stoger, E., Ma, J. K. C., Fischer, R., Christou, P. (2005) Sowing the seeds of success: Pharmaceutical proteins from plants. *Curr. Opin. Biotechnol.* **16**, 167–173.

Strasser, R., Altmann, F., Steinkellner, H. (2014) Controlled glycosylation of plant-produced recombinant proteins. *Curr. Opin. Biotechnol.* **30**, 95–100.

Strasser, R., Stadlmann, J., Schähs, M., Stiegler, G., Quendler, H., Mach, L., Glössl, J., Weterings, K., Pabst, M., Steinkellner, H. (2008) Generation of glyco-engineered Nicotiana benthamiana for the production of monoclonal antibodies with a homogeneous human-like N-glycan structure. *Plant Biotechnol. J.* **6**, 392–402.

Tschofen, M., Knopp, D., Hood, E., Stöger, E. (2016) Plant Molecular Farming: Much More than Medicines. *Annu. Rev. Anal. Chem.* **9**, 271–294.

Turk, B. (2006) Targeting proteases: Successes, failures and future prospects. *Nat. Rev. Drug Discov.* **5**, 785–799.

Twyman, R. M., Schillberg, S., Fischer, R. (2013) Optimizing the yield of recombinant pharmaceutical proteins in Plants. *Curr. Pharm. Des.* **19**, 5486–5494.

Twyman, R. M., Stoger, E., Schillberg, S., Christou, P., Fischer, R. (2003) Molecular farming in plants: Host systems and expression technology. *Trends Biotechnol.* **21**, 570–578.

Walker, L. M., Phogat, S. K., Chan-Hui, P. Y., Wagner, D., Phung, P., Goss, J. L., Wrin, T., Simek, M. D., Fling, S., Mitcham, J. L., Lehrman, J. K., Priddy, F. H., Olsen, O. A., Frey, S. M., Hammond, P. W., Protocol, G., Kaminsky, S., Zamb, T., Moyle, M., Koff, W. C., Poignard, P., Burton, D. R., Investigators, P. G. P., Kaminsky, S., Zamb, T., Moyle, M., Koff, W. C., Poignard, P., Burton, D. R. (2009) Broad and potent neutralizing antibodies from an African donor reveal a new HIV-1 vaccine target. *Science* **326**, 285–289.

Walsh, G. (2010) Post-translational modifications of protein biopharmaceuticals. *Drug Discov. Today* **15**, 773–780.

Ward, A. B., Wilson, I. A. (2015) Insights into the trimeric HIV-1 envelope glycoprotein structure. *Trends Biochem. Sci.* **40**, 101–107.

West, A. P., Scharf, L., Scheid, J. F., Klein, F., Bjorkman, P. J., Nussenzweig, M. C. (2014) Structural insights on the role of antibodies in HIV-1 vaccine and therapy. *Cell* **156**, 633–648.

Wu, X., Yang, Z.-Y., Li, Y., Hogerkorp, C.-M., Schief, W. R., Seaman, M. S., Zhou, T., Schmidt, S. D., Wu, L., Xu, L., Longo, N. S., Mckee, K., O'Dell, S., Louder, M. K., Wycuff, D. L., Feng, Y., Doria-Rose, N., Connors, M., Kwong, P. D., Roederer, M., Wyatt, R. T., Nabel, G. J., Mascola, J. R. (2010) Rational design of envelope identifies broadly neutralizing human monoclonal antibodies to HIV-1. *Science* **329**, 856–861.

Zhang, Z., Li, S., Gu, Y., Xia, N. (2016) Antiviral therapy by HIV-1 broadly neutralizing and inhibitory antibodies. *Int. J. Mol. Sci.* **17**, 1901.

Zhou, T., Georgiev, I., Wu, X., Yang, Z.-Y., Dai, K., Finzi, A., Kwon, Y. Do, Sheid, J. F., Shi, W., Xu, L., Yang, Y., Zhu, J., Nussenzweig, M. C., Sodorski, J., Shapiro, L., Nabel, G. J., Mascola, J. R., Kwong, P. D. (2010) Structural basis for broad and potent neutralization of HIV-1 by antibody VRC01. *Science (80-.).* **329**, 811–817.

Zhou, T., Lynch, R. M., Chen, L., Acharya, P., Wu, X., Doria-Rose, N. A., Joyce, M. G., Lingwood, D., Soto, C., Bailer, R. T., Ernandes, M. J., Kong, R., Longo, N. S., Louder, M. K., McKee, K., O'Dell, S., Schmidt, S. D., Tran, L., Yang, Z., Druz, A., Luongo, T. S., Moquin, S.,

Srivatsan, S., Yang, Y., Zhang, B., Zheng, A., Pancera, M., Kirys, T., Georgiev, I. S., Gindin, T., Peng, H. P., Yang, A. S., Mullikin, J. C., Gray, M. D., Stamatatos, L., Burton, D. R., Koff, W. C., Cohen, M. S., Haynes, B. F., Casazza, J. P., Connors, M., Corti, D., Lanzavecchia, A., Sattentau, Q. J., Weiss, R. A., West, A. P., Bjorkman, P. J., Scheid, J. F., Nussenzweig, M. C., Shapiro, L., Mascola, J. R., Kwong, P. D. (2015) Structural repertoire of HIV-1-neutralizing antibodies targeting the CD4 supersite in 14 donors. *Cell* **161**, 1280–1292.

Zolla-Pazner, S., Cardozo, T. (2010) Sequence-variable regions provide a paradigm for vaccine design. *Nat Rev Immunol* **10**, 527–535.

APPENDIX

LIST OF ABBREVIATIONS

Abs	absorbance
Ab	antibody
ABPP	activity-based probe profiling
Ac-YVAD-CMK	N-acetyl-tyrosyl-valyl-alanyl-aspartyl chloromethyl ketone
ADCC	antibody-dependent cellular cytotoxicity
AEBSF	4-(2-aminoethyl)benzenesulfonyl fluoride hydrochloride
AF	apoplastic fluid
AIDS	acquired immunodeficiency syndrome
A. tumefaciens	*Agrobacterium tumefaciens*
biotinyl-YVAD-CMK	biotinyl-tyrosyl-valyl-alanyl-aspartyl chloromethyl ketone
bnAbs	broadly neutralizing antibodies
bp	base pairs
BSA	bovine serum albumin
CaMV	Cauliflower mosaic virus
CCR5	C-C chemokine receptor type 5
CDR(H)	complementarity-determining region (heavy chain)
CD4 (bs)	cluster of differentiation 4 (binding site)
$C_{H/L}$	constant heavy/light
CHO	Chinese hamster ovary
CPMV	Cowpea mosaic virus
CRISPR	clustered regularly interspaced short palindromic repeats
CXCR4	C-X-C chemokine receptor type 4
ddW	double-distilled water
DMSO	dimethyl sulfoxide
DNA	deoxyribonucleic acid
dNTPs	deoxynucleotide triphosphates

DTT	dithiothreitol
E. coli	*Escherichia coli*
Env	HIV envelope glycoprotein
ER	endoplasmic reticulum
Fab	fragment antigen-binding
Fc	fragment crystallizable
FP-biotin	fluorophosphonate-biotin
FT	flow-through
Fw	forward
GA	Gibson assembly
Gen	gentamycin
GMP	good manufacturing practice
gp	glycoprotein
hc	heavy chain
HF	high fidelity
HIV-1	human immunodeficiency virus type 1
HPLC	high performance liquid chromatography
HRP	horseradish peroxidase
HT	hypertrans
Ig	immunoglobulin
kDa	kilodalton
Kan(R)	kanamycin (resistance)
LB	lysogeny broth
lc	light chain
LC	liquid chromatography
mAb	monoclonal antibody
MES	2-(N-morpholino)ethanesulfonic acid
MS	mass spectrometry
Nb	*Nicotiana benthamiana*
N. benthamiana	*Nicotiana benthamiana*

Neo(R)	neomycin (resistance)
nos	nopaline synthase
OD	optical density
PCR	polymerase chain reaction
PCD	programmed cell death
PMSF	phenylmethylsulfonyl fluoride
PNGase F	peptide-N-glycosidase F
PTM	posttranslational modification
Q-TOF	quadrupole time-of-flight
rcf	relative centrifugal force
RNA	ribonucleic acid
RNAi	RNA interference
rpm	revolutions per minute
Rv	reverse
SARS	severe acute respiratory syndrome
SBT	subtilase
SDS	sodium dodecyl sulfate
SOC	super optimal broth with carbon catabolite repression
TAE	tris-acetate-EDTA
TALEN	transcription activator-like effector nuclease
TBSV	Tomato bushy stunt virus
T-DNA	transfer DNA
TEMED	tetramethylethylenediamine
Tris	tris(hydroxymethyl)aminomethane
$V_{H/L}$	variable heavy/light
UTR	untranslated region
Z-VAD-FMK	benzyloxycarbonyl-valyl-alanyl-aspartyl fluoromethyl ketone
ZFN	zinc finger nuclease
6xHis-tag	hexahistidine-tag

STATEMENT OF ORIGINALITY

This is to certify, that the intellectual content of this thesis is the product of my own independent and original work and that all the sources used in preparing this thesis have been duly acknowledged.

Ana Vrkić